Postprint: Liu Huang, et al., Separation and Purification Technology, 297, 2022, 121504
https://doi.org/10.1016/j.seppur.2022.121504

Polymeric membranes and their derivatives for H_2/CH_4 separation: state of the art

Liu Huang[1], Ziman Xing[1], Xinyi Zhuang[1], Jing Wei[1,2,3,4], Yulei Ma[1,2,3,4], Bangda Wang[1,2,3,4], Xia Jiang[1,2,3,4], Xuezhong He[5], Liyuan Deng[6], Zhongde Dai[1,2,3,4]*

[1]College of Architecture and Environment, Sichuan University, Chengdu 610065, China
[2]National Engineering Research Centre for Flue Gas Desulfurization, Chengdu 610065, China
[3]Carbon Neutral Technology Innovation Center of Sichuan, Chengdu 610065, China
[4]School of Carbon Neutrality Future Technology, Sichuan University, Chengdu 610065, China
[5]Department of Chemical Engineering, Guangdong Technion - Israel Institute of Technology, 241 Daxue Road, Shantou, Guangdong, 515063, China
[6]Department of Chemical Engineering, Norwegian University of Science and Technology Trondheim, 7491, Norway
*Corresponding Author:
Zhongde Dai: zhongde.dai@scu.edu.cn

Abstract:

The hydrogen economy becomes an important route in approaching carbon neutrality. Compared to conventional methods, membrane separation possesses combined merits, including energy-saving, convenience, and economic efficiency. In the past few years, significant progress has been made in hydrogen (H_2)/methane (CH_4) separation membranes, but a systematic review of membrane materials for this application is still lacking. Herein, the research progress of polymeric membranes, mixed matrix membranes (MMMs), and carbon molecule sieve (CMS) membranes has been critically reviewed and discussed. Research results from the latest literature are summarized and analyzed. It is found that polymeric membranes and CMS membranes exhibit outstanding H_2/CH_4 separation properties, while MMMs, although widely investigated, show lower performance. The perspectives and future research directions for H_2/CH_4 separation membranes were presented. This review provides an in-depth understanding of the latest research and offers valuable inspirations for theoretical research and practical applications for the H_2/CH_4 separation membranes.

Key words:

Membrane separation; hydrogen; methane; mixed matrix membranes; carbon molecular sieve membranes;

TOC:

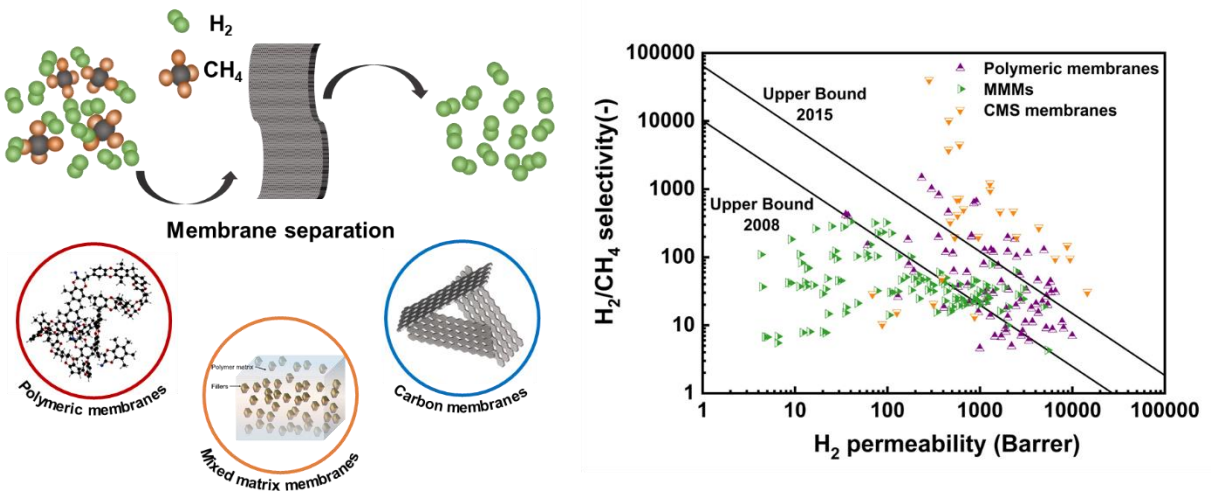

1. Introduction

1.1 Carbon neutrality

Global warming, caused by the excessive consumption of fossil fuels, has been bringing about a series of climate and environmental problems, such as glacier retreat, sea-level rise, ocean acidification, species extinction, loss of biodiversity, and extreme climate (e.g., drought, flood, wildfires) [1, 2]. Carbon dioxide (CO_2) concentration in the air increased to a high value that had never existed in history [3, 4]. For the sustainable development of human society, more than 100 countries have actively responded to the ultimate goal of zero-carbon by controlling carbon emissions [5]. China has proposed to reach a carbon peak by 2030 and accomplish carbon neutrality by 2060 [6].

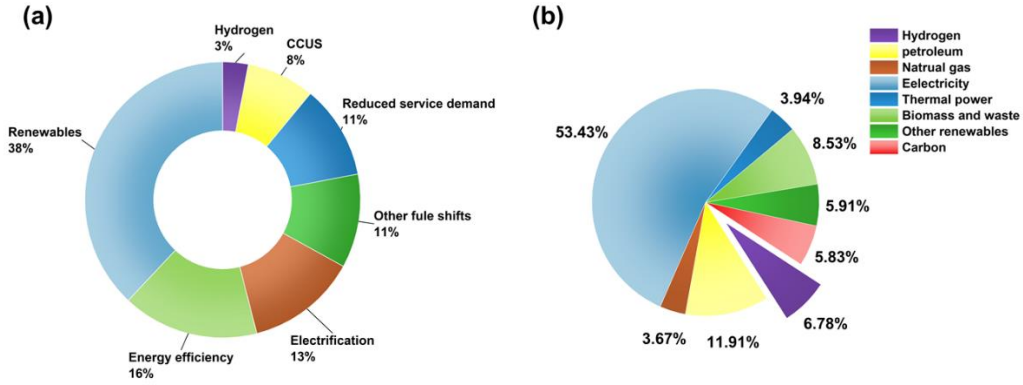

Figure 1. (a) Solutions to reduce carbon emission and their contribution [6]. (b). The estimated energy demand for different sectors in China in 2060 [6].

As shown in **Figure 1a**, there are several ways to reduce carbon emissions, including using renewable energy, improving energy efficiency, electrification, developing hydrogen energy, as well as carbon capture, utilization and storage (CCUS) [7]. Among these solutions, using renewable energy is considered the most important part as it will account for 38% of carbon emissions reduction before 2060. Afterwards, improving energy efficiency, electrification, shifting fuels and reducing service demand could also reduce carbon emissions significantly. CCUS will contribute around 8% to the total carbon emissions reduction. It is estimated that hydrogen energy will account for around 3% of the total carbon emissions reduction. However, according to IEA's

prediction [8], H_2 consumption will increase to ~520 Mt per year in the 2070s, which is 7 times higher than that in 2020. H_2 will play a big role in synfuel production, transportation, and power supply. Its high energy to mass ratio makes it particularly suitable for heavy-duty, long-distance road freight, maritime and aviation applications. Furthermore, H_2 is critical for replacing coal and gas in fossil fuel intensive industrial processes such as steelmaking. In addition, as **Figure 1b** shows, H_2 will account for 6.78% of the total energy demand in 2060 under China's commitment target scenario. Hence, H_2 is of vital significance for achieving carbon neutrality and sustainable development.

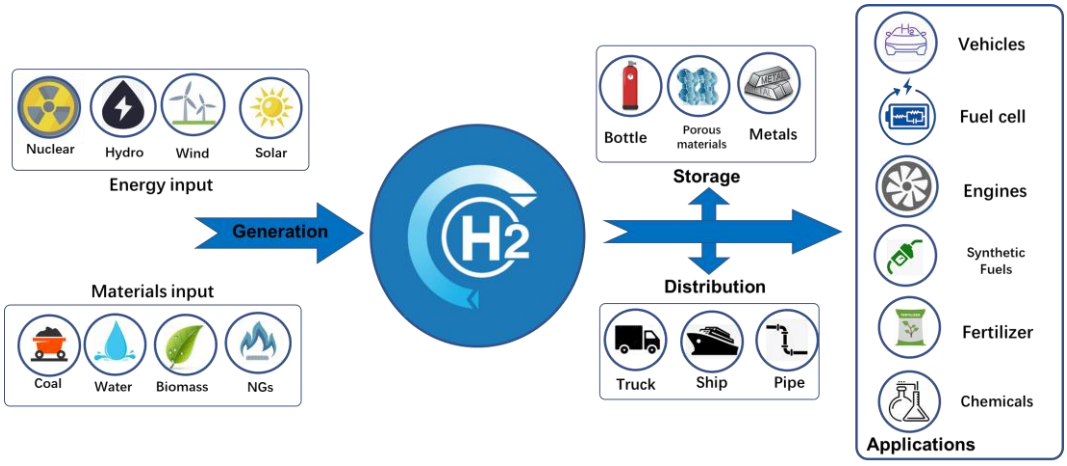

Figure 2. Hydrogen economy.

1.2 Hydrogen economy

Hydrogen, the first element in the periodic table, has a colorless, odorless physical property and is a highly flammable gas. Since the early 1920s, H_2 has been used as fuel in combustion engines, and then in the 1960s, it was used in lunar rockets. As a combustion material, H_2 has several times higher combustion efficiency than fossil fuels [9, 10]. The hydrogen economy consists of four processes: generation, storage, distribution and application. The details are shown in **Figure 2**. The H_2 market is now much larger than ever and is estimated to grow to 154 billion USD in 2022 [11]. The supply of clean energy is intrinsically related to zero carbon emission, and the key factors that determine whether the two can fit perfectly include economic strength,

relevant policies, and environmental ontology [12].

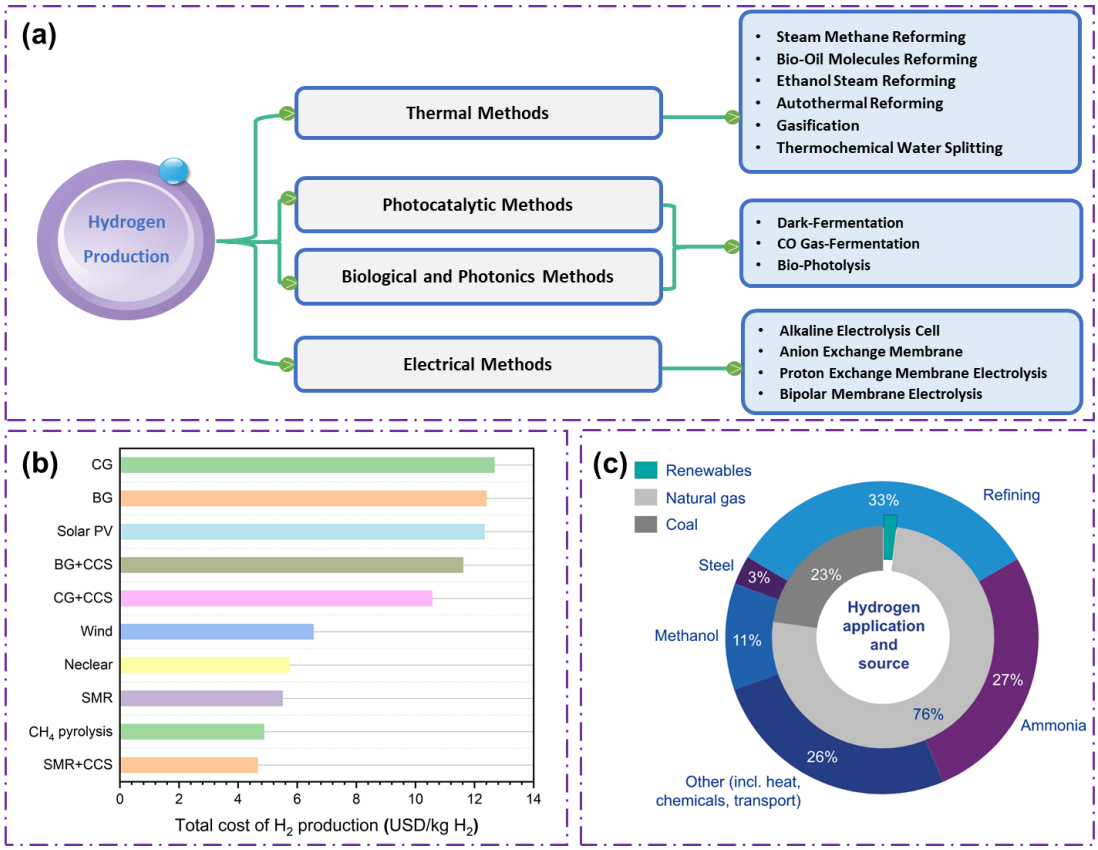

Figure 3. (a) H_2 production methods, (b) the accessed cost of H_2 produced via various methods [13], and (c) H_2 production capacity[14].

As it combines readily with other elements, hydrogen does not occur as a stand-alone gas and therefore must be extracted from other sources. As shown in **Figure 3a**, thermal, photocatalytic, biological, photonic and electrical methods can be applied in H_2 production. Photocatalysis uses solar energy to split water to produce H_2 and does not need to consume fossil fuels, but its low H_2 production efficiency, harsh reaction conditions and high sacrificial agent cost hinder its further application. The biological and photon method, which uses biomass as resources to produce H_2, is relatively economical compared to the photocatalysis process. The last method is to produce H_2 mainly by electrolysis water in an electrolytic cell. If low-cost electricity can be applied, electrolysis of water will be a promising method for large-scale H_2 production despite there being some technical problems that need to be solved [7, 10].

Although there are many new H_2 production methods, the thermochemical process is still the most effective and most widely selected method for H_2 production (around 96% of H_2 is produced from fossil fuels) [10]. The thermochemical process includes reforming, gasification, and thermochemistry [5, 8]. At present, fossil fuels (natural gas: 48%, heavy oils and naphtha: 30%, and coal: 18% [15]) are the most commonly used source of H_2 production, and natural gas reforming is the most economical method. In the reforming process [4], hydrocarbons and steam react with each other to convert into H_2 and CO_2, and synthesis gas production is an intermediate step. CO in synthesis gas reacts with water vapor via the water gas shift (WGS) reaction and enhances H_2 yield.

Figure 3b lists the assessed cost of the H_2 produced via various methods[13]. Obviously, SMR (steam methane reforming) with CCS (carbon capture and storage) is the most cost-effective, with a cost of around 4.66 USD per kg H_2. Coal gasification (CG), biomass gasification (BG) and electrolysis from solar photovoltaic energy (solar PV) are three most expensive production routes, all of whic cost about 12 USD per kg H_2. As can be seen from **Figure 3c** [14], the total H_2 production is mainly from fossil fuels, with 76% of the H_2 coming from natural gas and 23% from coal. Only ~2% of the global H_2 production stems from renewables.

As clearly indicated in **Figure 3c**, in the near future, H_2 will mainly come from fossil fuel related processes, such as natural gas steam reforming, petrochemical refinery, purge gas recovery and so on [16]. H_2 /CH_4 separation is one of the critical steps in these H_2 production processes. Furthermore, the transportation of H_2 still faces a great challenge now. Injecting H_2 into the natural gas grid could be a potential solution, but recovering H_2 from the natural gas grid for end users requires energy-efficient technologies to bring down the H_2 production cost.

Compared to conventional separation technology (e.g., sorption), membrane separation possesses many advantages like convenient operation, low cost and energy consumption, which endows its bright prospects. In the past few years, many different membrane materials have been developed for H_2/CH_4 separation, including metal membranes, microporous inorganic membranes, polymeric membranes and their

derivatives. Metal membranes (e.g., Palladium membranes) are well-known for their ultrahigh selectivity, which is perfect for producing H_2 with high purity. However, their high cost and low poisoning resistance hinder their wide application. Microporous inorganic membranes (e.g., Zeolite and ceramic) have been also intensively studied for H_2 separation due to their excellent molecule seiving, which normally results in H_2/CH_4 separation performance well above the Upper Bound. In addition, most inorganic membranes present better chemical and mechanical properties compared to polymeric membranes. However, their complicated fabrication procedure and relatively high cost are the bottleneck for their further industrialization. On the other hand, compared to inorganic membranes, polymeric membranes have much better processibility and lower price, which ensures that polymeric membranes can be fabricated into thin-film-composite membranes with a thin selective layer at a low cost. In addition, polymeric membranes also hold the potential for further functionalization, not only for polymer chain itself, but also for polymeric matrix.

Even though there is an excellent review on microporous membranes for H_2/CH_4 separation [17], the polymeric membranes and their derivatives for H_2/CH_4 separation have not been systematically analyzed. Therefore, this work expounds on the recent progress on H_2/CH_4 separation polymeric membranes and their derivatives. The pros and cons of polymeric membranes, MMMs, and CMS membranes are systematically discussed. Future perspectives of the H_2/CH_4 separation were also proposed.

2. General background for H_2 separation membranes

Membranes can be defined as physical barriers that allow selective transport of a large number of species and are widely used for separation and purification in various industries [18]. Many membranes have been developed for H_2 separation, including polymeric membranes [19], MMMs [20-24], CMS membranes [25] and inorganic membranes [26]. In H_2 gas transport mechanisms varies in different membranes, thus the transport in different membranes is briefly discussed.

2.1 H_2 transport in membranes

Several mechanisms can be used to describe H_2 transport in gas separation membranes (as shown in **Figure 4** [2]). The most commonly used theoretical model in dense membranes is the solution-diffusion model, which consists of three main steps: adsorption at the upstream boundary (feed side), diffusion through the membrane, and desorption on the downstream side (permeate side) [27]. In porous membranes, based on the pore size, transportation and separation of H_2 molecules can be described using laminar flow, Knudsen diffusion or molecular sieve separation. In practical applications, molecular sieving and solution-diffusion are the most common separation mechanisms for porous and dense membranes, respectively.

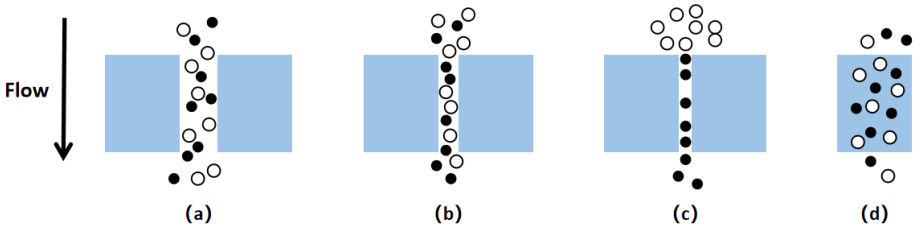

Figure 4. H_2 transport mechanism in porous and dense membranes: (a) laminar flow; (b) Knudsen diffusion; (c) molecular sieving; (d) solution-diffusion.

2.2 Process parameters in membrane separation

Gas permeability (P_i, also named permeation coefficient) and ideal selectivity (α_{ij}^*) are two key parameters to evaluate the intrinsic properties of gas separation membrane materials, gas permeability can be expressed as shown in equation (1):

$$P = D \times S = \frac{Ql}{(p_2 - p_1)A} = \frac{22414}{A} \frac{V}{RT} \frac{l}{(p_2 - p_1)} \frac{dp}{dt} \quad (1)$$

where P is the permeability (cm^3(STP) cm cm^{-2} s^{-1} $cmHg^{-1}$), D is diffusion coefficient (cm^2 s^{-1}), S is solubility coefficient, A is the membrane area (cm^2), V is the constant volume of the permeate side (cm^3), Q is the permeating flow rate (cm^3 (STP) s^{-1}), R is the universal gas constant (6236.56 cm^3 cmHg mol^{-1} K^{-1}), T is the absolute operating temperature (K), l is the membrane thickness (cm), p_2 and p_1 are the feed pressure and

permeate pressure (cmHg) respectively, and *dp/dt* is the rate of pressure increase on the permeate side (cmHg s^{-1}) [28].

Ideal selectivity (α_{ij}^*) is usually obtained from single gas permeation tests and it is defined as the permeability ratio between the more permeable gas (i) and less permeable one (j), or as the product of diffusivity selectivity and solubility selectivity as shown in equation (2):

$$\alpha_{ij}^* = \frac{P_i}{P_j} = \left(\frac{D_i}{D_j}\right)\left(\frac{S_i}{S_j}\right) \quad (2)$$

Where P_i and P_j are the permeability of gas species i and j in the membrane, respectively [29].

In addition, permeance (Q_i, also known as normalized flux) is usually used to evaluate the performance of structurally complex asymmetric or composite membranes. Gas permeance can be expressed as equation (3):

$$Q_i = \frac{J_i}{\Delta p \cdot A} = \frac{P_i}{l} \quad (3)$$

In mixed gas permeation tests, there may be interaction and/or competition between different gases, so the actual separation factor is not always equal to the ideal selectivity. And the concentration polarization and membrane plasticization during actual separation normally lead to greater differences between separation factor and ideal selectivity. The separation factor is calculated by the composition ratio of permeate gas to feed gas, which can be expressed as equation (4):

$$\alpha_{ij} = \frac{y_i / x_i}{y_j / x_j} \quad (4)$$

Where y_i and y_j are the molar fraction of gas species i and j on the permeate side, while x_i and x_j are the molar fraction of gas species i and j on the feed side. Unlike permeability (P_i) and idea selectivity (α_{ij}^*), permeance (Q_i) and separation factor (α_{ij}) are more sensitive to operating conditions such as the ratio of pressure in feed and permeate sides, stage-cut, etc. The separation factor (α_{ij}) can approach the ideal selectivity (α_{ij}^*) when the partial pressure on the feed side is much higher than that on the permeate side (as shown in equation (5)) [29].

$$\alpha_{ij}=\frac{y_i/y_j}{x_i/x_j}=\frac{1}{x_i/x_j}\frac{P_i}{P_j}\frac{(p_{f,i}-p_{p,i})}{(p_{f,j}-p_{p,j})}\approx\frac{P_i}{P_j}=\alpha_{ij}^{*} \quad (5)$$

Many different units are used to represent permeation results. For the convenience of the readers, all the gas permeability and gas permeance units used in this work are converted to Barrer (1 Barrer = 10^{-10} cm^3(STP) cm cm^{-2} s^{-1} $cmHg^{-1}$) and GPU (1 GPU = 10^{-6} cm^3(STP) cm^{-2} s^{-1} $cmHg^{-1}$), respectively. The most commonly used unit for gas permeance is the gas permeation unit (GPU). However, other units are also widely used. Conversion rates between different units are shown in **Table 1** [29].

Table 1. Gas permeance units conversion [29].

	(GPU)10^{-6} cm^3(STP) cm^{-2} s^{-1} $cmHg^{-1}$	10^{-7} cm^3(STP) cm^{-2} s^{-1} kPa^{-1}	10^{-10} mol m^{-2} s^{-1} Pa^{-1}	10^{-3} m^3(STP) m^{-2} h^{-1} bar^{-1}
(GPU)10^{-6} cm^3(STP) cm^{-2} s^{-1} $cmHg^{-1}$	1	7.50	3.35	2.70
10^{-7} cm^3(STP) cm^{-2} s^{-1} kPa^{-1}	0.133	1	0.447	0.360
10^{-10} mol m^{-2} s^{-1} Pa^{-1}	0.299	2.24	1	0.806
10^{-3} m^3(STP) m^{-2} h^{-1} bar^{-1}	0.365	2.78	1.24	1

3. Advances in polymeric membranes for H_2/CH_4 separation

Till now, polymeric membranes have been extensively studied for gas separation because of their prominent merits that inorganic membranes lack, *i.e.,* convenient fabrication and low cost [30]. However, polymeric membranes suffer from a trade-off between their permeability and selectivity, which is well-known as the Robeson upper bound [31]. In 1999, Freeman et al. developed a theory regarding the improvement of polymeric membrane performance, suggesting that (1) increased backbone stiffness and interchain separation and (2) enhanced solubility selectivity should be achieved to

outperform the famous upper bounds [32].

Due to the relatively large difference in molecule weight (H_2-2 g/mol, CH_4-16 g/mol) and size (H_2-0.289 nm, CH_4-0.384 nm), H_2 and CH_4 present a rather different solubility in polymeric membranes. In most cases, H_2 diffusivity dominates the overall H_2 permeability, thus most of the research works focusing on H_2/CH_4 separation were dedicated to improving H_2/CH_4 diffusion selectivity by introducing more bulky side groups onto rigid glassy polymeric main chains. Some of the representative polymers are polymers of intrinsic microporosity (PIMs), Tröger's base (TB) polymers and polyimides (PIs).

3.1 Application of PIMs

In 2004, Budd and co-workers introduced a new class of microporous polymers named PIMs [33, 34]. They are glassy, rigid, randomly contorted, and have no rotational freedom in the polymer backbone, thus having a large fractional free volume (*FFV*) [35]. Neat PIMs, like most high free volume polymers, present relatively high H_2 permeability accompanied by low H_2/CH_4 selectivity. However, the H_2/CH_4 selectivity of PIM-based membranes can be improved significantly by proper functionalization. **Table 2** lists the application of PIMs in the past few years on H_2/CH_4 separation membranes.

Table 2. H_2/CH_4 separation performances of PIMs-based self-standing membranes

Membrane materials	**P_{Feed} (bar)**	**T (°C)**	**P_{H_2} (Barrer)**	**α_{H_2/CH_4} (-)**	**Ref**
PIM-1	1.01	35	3380	5.9	[36]
PIM-NH_2	1.01	35	1450	6.8	
PIM-t-BOC	1.01	35	130	26	
PIM-deBOC (acid)	1.01	35	1700	6.7	
PIM-deBOC (thermal)	1.01	35	2000	13	
PIM-1	3.55	35	1912	7.99	[37]
PIM-1-400	3.55	35	914	648.23	

PIM-1-450	3.55	35	234	1472	
PIM-1-500	3.55	35	509	113.62	
PIM-1-550	3.55	35	997	4.54	
AOPIM-1	2	25	932	22	[38]
TX-AOPIM-1-280-48	2	25	1895	9	
TX-AOPIM-1-370-24	2	25	1320	127	
TX-AOPIM-1-390-24	2	25	455	455	
TX-AOPIM-1-390-48	2	25	300	1000	
CANAL-Me-Me_2F (1 d)	1	35	5200	9.0	[39]
CANAL-Me-Me_2F (72 d)	1	35	3300	116	
CANAL-Me-Me_2F (150 d)	1	35	2380	185	
CANAL-Me-S5F (1 d)	1	35	3700	11	
CANAL-Me- S5F (90 d)	1	35	2500	101	
CANAL-Me- S5F (150 d)	1	35	2000	193	
CANAL-Me-S6F (1 d)	1	35	3100	11	
CANAL-Me- S6F (31 d)	1	35	2900	8.0	
CANAL-Me- S6F (150 d)	1	35	2000	120	
CANAL-Me- DHP (1 d)	1	35	2800	7	
CANAL-Me- DHP (77 d)	1	35	1400	119	
CANAL-Me- DHP (158 d)	1	35	860	621	

Rodriguez et al. [36] reported an in-situ crosslinking and solid-state deprotection method to access sorption traits while retaining backbone benefits in microporous amine-functionalized PIM-1. The modification leads to increased free volume element (FVE) sizes and a preserved narrow FVE distribution, thus the mediocre polymers were able to outperform the H_2/CH_4 upper bound. Compared to PIM-NH_2, PIM-deBOC (acid) showed an enhanced permeability and a similar selectivity, while an increase both in H_2 permeability (from 1450 to 2000 Barrer) and H_2/CH_4 selectivity (from 6.8 to 13) was observed in PIM-deBOC (thermal).

He et al. [37] carried out an intermediate thermal manipulation on the PIM-1 membrane. When the membrane was treated at a temperature higher than 400 °C, it was found that

the overall H_2/CH_4 separation performance of the membranes were dramatically changed due to the synergistic effects of thermal-induced cross-linking and thermal decomposition. Treating the PIM-1 membrane at 400 °C resulted in a membrane presenting an H_2 permeability of 914 Barrer and an H_2/CH_4 selectivity of 648.2. Further increasing the temperature to 450 °C resulted in a lower permeability (234 Barrer) and higher selectivity (1472). However, an even higher temperature will make this trend in the opposite direction: higher permeability will be obtained with lower selectivity. This laterally evidences the importance of a precisely tuned pore size distribution of microporous polymers to improve gas separation performance [40, 41].

Huang et al. [38] also utilized the thermal cross-linking method to fabricate amidoxime-functionalized PIM-1 (AOPIM-1) membranes with supreme H_2 separation performance. By carefully controlling the annealing conditions, the pore structure of AOPIM-1 membranes could be tuned without destroying the polymeric main-chain structure. Like most polymeric membranes, increasing heat treatment temperature firstly led to an increase in H_2 permeability, but further increasing temperature resulted in decrement for all the tested gases. For H_2/CH_4 selectivity, membranes treated at a lower temperature of 280 °C presented a value (9) lower than the neat polymer (22), while a much higher selectivity (127) could be obtained at a higher thermal treatment temperature of 370 °C. In addition, results showed that high selectivity mainly came from diffusion selectivity, denoting the thermal treatment was mainly regulating its free volume elements (FVE) size and distributions. When optimized annealing temperature (390 °C) and duration time (48 h) was selected, the resultant TX-AOPIM-1 membrane with simultaneously high H_2 permeability (300 Barrer) and H_2/CH_4 selectivity (1000) were obtained, which surpassed the upper bound. Physical aging, which indicated reversible densification induced by the loss of the nonequilibrium free volume [42], was also investigated. After aged for 180 days, the TX-AOPIM-1 membrane had an imperceptible change in permeability but underwent apparent enhancement of selectivity.

Lai et al. [39] reported a series of hydrocarbon ladder polymer membranes that simultaneously achieved high selectivity and superior permeability. In their work, ladder polymers with high surface area and high thermal stability were prepared by catalytic arene-norbornene annulation (CANAL) polymerization process using ladder dinorbornenes Me_2F, S_5F, S_6F, DHP and p-dibromo-p-xylene as monomers. These membranes exhibited high permeability but only moderate selectivity when they were freshly prepared, but after aging, their separation performance improved remarkably due to sharply increased selectivity, as **Figure 5a** shows. For instance, after being aged for 150 days, although the H_2 permeability of the CANAL-Me-Me_2F membrane decreased from 5200 Barrer to 2380 Barrer, its H_2/CH_4 selectivity rose intensively from 9 to 185, which is over 20 times higher than the neat value. Such aging trends and performance improvement were not observed for 2D CANAL polymers with similar hydrocarbon structures, indicating the importance of ladder-chain configurations. Meanwhile, the physical aging of high free volume polymers is illustrated in **Figure 5b**. In most cases, physical aging leads to decreased permeability and increased selectivity. But sometimes, other circumstances can also be observed.

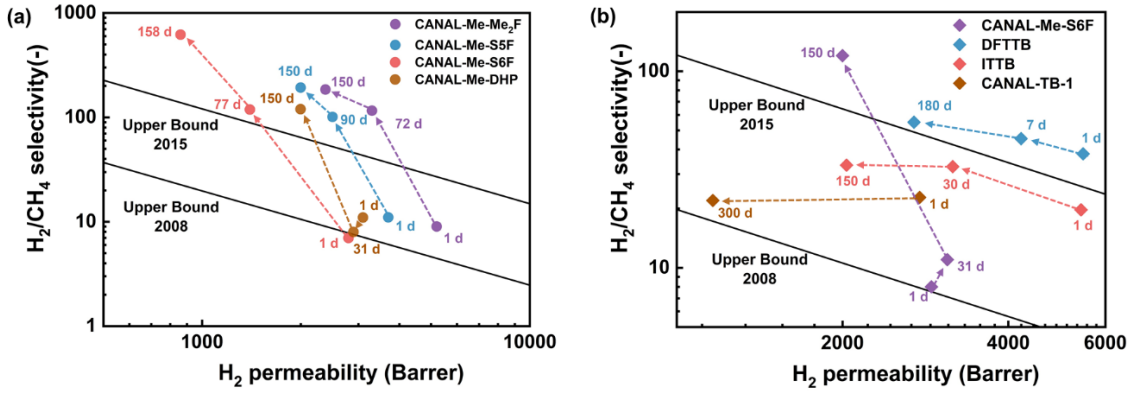

Figure 5. (a) The remarkable improvement of separation performance of CANAL-dihydrophenanthrene-based membrane after aging [39]. (b) Physical aging of representative high free volume polymers [39, 43-45].

3.2 Application of TB polymers

Employing Tröger's base (TB) as a backbone structure and triptycene as a building block has been widely employed to develop PIMs [43]. Table 3 lists the application of TB polymers in the past few years on H2/CH4 separation membranes.

Table 3. H_2/CH_4 separation performances of TB polymers-based self-standing membranes

Membrane materials	**P_{Feed} (bar)**	**T (°C)**	**P_{H_2} (Barrer)**	**α_{H_2/CH_4} (-)**	**Ref**
DFTTB	2	-	5468	38.0	[43]
DFTTB Aged 7 days	2	-	4220	45.4	
DFTTB Aged 180 days	2	-	2696	55.0	
CTTB	2	35	5257	26.3	[44]
MTTB	2	35	5897	30.2	
ITTB	2	35	5423	19.7	
ITTB Aged 30 days	2	35	3171	32.7	
ITTB Aged 150 days	2	35	2034	33.3	
PIM-SBI-TB	1	25	2200	4.9	[46]
PIM-EA-TB	1	25	7760	11.1	
PIM-trip-TB	1	25	8039	8.9	[47]
PIM-trip-TB Aged 100 days	1	25	4740	21.7	
PIM-Btrip-TB	0.1-1.3	25	9980	6.93	[48]
PIM-Btrip-TB Aged 166 days	0.1-1.3	25	4280	15.1	
PIM-MP-TB	1	25	4050	20.3	[49]
PIM-TMN-Trip-TB	1	25±1	6100	8.6	[50]
PIM-BM/TB	3.45	35	1925	17.2	[51]
PIM-BM/TB (80°C-20h)	3.45	35	1392	29.6	
PIM-BM/TB (200°C-20h)	3.45	35	721	60.1	
PIM-BM/TB (250°C-20h)	3.45	35	356	197.7	
PIM-BM/TB (250°C-5h)	3.45	35	582	36.4	
PIM-BM/TB (250°C-10h)	3.45	35	427	118.6	
PIM-BM/TB (300°C-5h)	3.45	35	358	813.6	

CANAL-TB-1	2	35	2760	22.8	[45]
CANAL-TB-1Aged 300 days	2	35	1163	22.0	
CANAL-TB-2	2	35	3608	17.6	
CANAL-TB-2Aged 300 days	2	35	2452	19.1	

Figure 6a illustrates the internal free volume (IFV) of triptycene and a representative structure of triptycene-containing TB-based ladder PIMs. To explore the effect of different regioisomers on the gas separation properties of TB-based ladder PIM membranes, Zhu et al. [44] developed three TB-based polymer membranes with triptycene groups, CTTB (from Trip-2,6-diamine), MTTB (from Trip-2,7-diamine), and ITTB (from 50/50 mixed Trip-2,6-diamine/Trip-2,7-diamine). Enhanced thermal stability, mechanical property, and microporosity were observed in the resulting membranes. Superior H_2 permeability and high H_2/CH_4 selectivity make CTTB and MTTB membranes both surpassed the 2015 upper bound for H_2/CH_4 separation ($P(H_2)$ =5275 Barrer and $\alpha(H_2/CH_4)$ =26.3 for CTTB; $P(H_2)$ =5897 Barrer and $\alpha(H_2/CH_4)$ =30.2 for CTTB). In the same year, a novel 2,3-difluoro-substituted 2,6(7)-triptycene diamine (DFTrip) monomer was designed and used to synthesize TB polymer (DFTTB) and prepare membranes. An H_2 permeability of 5468 Barrer and an H_2/CH_4 selectivity of 38 were obtained for the fresh TB membrane. Physical aging resulted in a decline in H_2 and CH_4 permeability together with an improved H_2/CH_4 selectivity [43], but still, the excellent gas separation performance was close to or surpassed the 2015 upper bound. The chemical structures of CTTB, MTTB, ITTB and DFTTB are shown in **Figure 6b**.

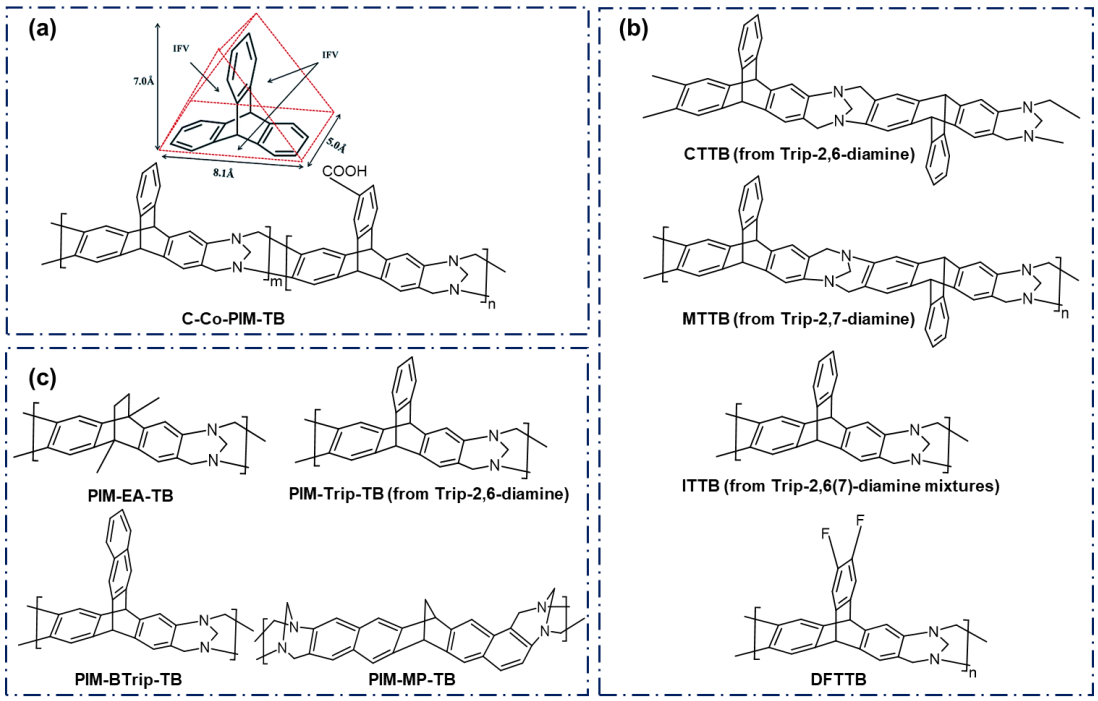

Figure 6. (a) Illustration of the internal free volume (IFV) of triptycene and a representative structure of triptycene-containing TB-based ladder PIMs. (b) Chemical structure of CTTB, MTTB, ITTB and DFTTB. (c) Chemical structure of several PIM-TB polymers.

Replacing the dioxin-like ring system in polymers with stiffer bridged bicyclic ring systems (e.g., ethanoanthracene (EA)) and designing polymers with greater shape-persistence are anticipated to improve the membrane properties. McKeown and coworkers [46] hypothesized that developing TB polymers with bridged bicyclic linking groups and greater shape-persistence is an efficient way to improve gas separation properties. In their work, rigid ethanoanthracene-based TB polymer (PIM-EA-TB) and flexible spirobisindane-based TB polymer (PIM-SBI-TB) were successfully synthesized. With enhanced microporosity, PIM-EA-TB had a particularly high H_2 permeability (up to 7760 Barrer) while the H_2 permeability of PIM-SBI-TB with soft segments was quite lower (2200). H_2/CH_4 selectivity of PIM-EA-TB was 11.1, which was also higher than that of PIM-SBI-TB (4.9). Performed as a molecular sieve, PIM-EA-TB showed an unrivalled potential for H_2 separation from CH_4.

Later on, the same group reported the properties of a novel triptycene-based PIM (PIM-Trip-TB) prepared via Tröger's base formation, which exhibited further enhancement

of separation performance for H_2/CH_4 and improved mechanical strength [47]. In this work, H_2 permeability was up to 8039 Barrer with an H_2/CH_4 selectivity of 12.8 at 25 °C and 1 bar, which well surpassed the 2008 Robeson upper bound. Even though attempts were made to reverse the effects of physical aging by soaking membranes with methanal, a 41% reduction of permeability and a corresponding enhancement of selectivity from 8.9 to 21.7 was observed on membranes aged for 100 days.

Later, monomers with higher rigidity were utilized to enhance the free volume, and the resultant PIM-BTrip-TB membranes showed exceedingly high H_2 permeability (9980 Barrer) and moderate H_2/CH_4 selectivity (6.93) [48]. Similarly, after being aged for166 days, the H_2 permeability of the PIM-BTrip-TB membrane decreased to 4280 Barrer while selectivity rose to 15.1. Later, this group applied 6,13-dihydro-6,13-methanopentacene (MP) hydrocarbon to further enhance the rigidity of TB-based PIM [49]. An H_2 permeability of 4050 Barrer and selectivity of 15.3 was obtained for the PIM-MP-TB membrane, the higher H_2/CH_4 selectivity may derive from its fewer interconnected pores. It is worth mentioning that its synthesis process was accomplished in only four simple steps from a cheaply available starting material, 4-nitro-o-xylene. The structures of these PIM-TB polymers with high separation performance can be seen in **Figure 6c**.

McKeown's group also constructed a 2D ribbon-shaped polymer (PIM-TMN-Trip) with a triptycene-based monomer which contains a fused tetramethyltetrahydronaphthalene (TMN) unit as the extended substituent. The TMN substituent endowed the polymer with solubility in organic solvents and enhanced intrinsic microporosity [50]. The PIM-TMN-Trip-TB membrane displayed an H_2 permeability of 6100 Barrer and an H_2/CH_4 selectivity of 8.6 while the PIM-TMN-Trip membrane demonstrated an ultrahigh H_2 permeability (16900 Barrer) together with an H_2/CH_4 selectivity of 4.95.

Chen et al. [51] novelly designed polymeric molecular sieve membranes with a multi-covalent-crosslinking method. They chose blended bromomethylated PIMs (PIM-BM) and TB, simultaneously providing inter- and intra-molecular crosslinking reaction sites

and enabling high permeability and selectivity. Reaction temperature, reaction time and the oxygen concentration were adjusted to tailor the pore structure and separation performance of the membranes. As the crosslinking temperature increased from 80 to 300 °C, the H_2 permeability decreased from 1392 Barrer to 358 Barrer while the H_2/CH_4 selectivity increased from 29.6 to 813.6. At 250 °C, increasing crosslinking time from 5h to 20 h also led to a reduction in gas permeability (from 582 Barrer to 356 Barrer) together with an increase of H_2/CH_4 selectivity (from 36.4 to 197.7). Besides, the oxygen concentration was a critical element and the H_2 gas permeability decreased but H_2/CH_4 selectivity floated up and down when increasing oxygen concentration. After physical ageing of over 360 days, H_2 permeability silghtly decreased and H_2/CH_4 selectivity increased from 100 to >300. Additionaly, the degree of bromomethlyation and the blending ratio of PIM-BM to TB can be controlled to futher tune the physical and gas separation properties of membranes developed in this work.

Ma et al. [45] reported two ladder polymers, CANAL-TBs, by fusing catalytic arene-norbornene annulation (CANAL) and TB motifs. Facile synthesis and high yielding were achieved by only two steps from commercially available starting materials, p-bromoanilines and norbornadiene. Both polymers exhibited mechanical flexibility and abundant micropores (11~15 Å) and ultramicropores (<7 Å). Freshly prepared CANAL-TB-1 and CANAL-TB-2 membranes exhibited an H_2 permeability of 2760 and 3608 Barrer and H_2/CH_4 selectivity of 22.8 and 17.6, respectively. After being aged for 300 days, both membranes experienced a great decline in permeability, but an increase in selectivity of CANAL-TB-2 was observed while CANAL-TB-1 showed a decrease in selectivity. Ultimately, all the CANAL-TBs membranes surpassed the 2008 upper bound for H_2/CH_4.

3.3 Application of PIs

Polyimides (PIs) with high free volume are also of great interest for H_2/CH_4 separation. Table 4 lists the application of PIs in the past few years on H2/CH4 separation

membranes.

Table 4. H_2/CH_4 separation performances of TB polymers-based self-standing membranes

Membrane materials	**P_{Feed} (bar)**	**T (°C)**	**P_{H_2} (Barrer)**	**α_{H_2/CH_4} (-)**	**Ref**
PI	1.01	35	963	15.5	[52]
PI-ABA (vapor method A)	1.01	35	35.4	417	
PI-ABA (vapor method B)	1.01	35	37.6	402.6	
6FDA-HTB	2	35	167	181	[53]
CTB1-DMN	2	35	1295	13.5	[54]
CTB1-DMN aged 60 days	2	35	759	21.0	
CTB2-DMN	2	35	1150	28.5	
CTB2-DMN aged 60 days	2	35	737	39.1	
6FDA-TrMCA	2.03	35	193	61	[55]
6FDA-TrMPD	2.03	35	407	18	
TPHI-TR-350	11.15	35	61	150	[56]
TPHI-TR-400	11.15	35	520	62	
TPHI-TR-450	11.15	35	810	200	
TPBO-0.25	3	35	1183	32	[57]
TPBO-0.75	3	35	1101	79	
TPBO-1.0	3	35	810	203	
TPBO-Ac-0.25	3	35	1701	43	
TPBO-Ac-0.75	3	35	1577	75	
TPBO-Ac-1.0	3	35	1123	125	
TAM-BDA-CMP@PSF	1	25	4924	126.3	[58]
TAM-DMTP-CMP@PSF	1	25	5808	43.3	
TAM-DBTP-CMP@PSF	1	25	6565	30.8	
POXINAR	2	35	170	77	[59]

Yoshioka et al. [52] modified a PI membrane with 4-aminobenzyl amine (ABA) vapor. The results show that the gas selectivity of amine-crosslinked PI membranes increased

exponentially with the increase of difference between the kinetic diameter of gases, and a 26 times higher H_2/CH_4 selectivity (417) was obtained, even though the H_2 permeability (35.4 Barrer) was much lower compared to the original PI membranes (963 Barrer).

Ma et al. [53] innovatively designed an OH-functionalized Tröger's base diamine, 1,7-diamino-6H,12H-5,11-methanodibenzo[1,5]diazocine-2,8-diol (HTB), which were used to synthesize two microporous PIs (PIM-PIs), 6FDA-HTB and SBI-HTB. The intrinsic hydrogen bounding in the hydroxyl-functionalized 6FDA-HTB membrane resulted in its intensive size-sieving ability, thus causing complimentary H_2/CH_4 selectivity (181) and a moderate H_2 permeability (167 Barrer). Two carbocyclic pseudo-TB-derived dianhydrides (CTB1 and its dione-substituted analogue, CTB2) were also synthesized to prepare PIM-PIs with dimethylnaphthidine (DMN) [54]. The obtained CTB1-DMN and CTB2-DMN both demonstrated good mechanical properties. CTB2-DMN displayed an H_2 permeability (1159 Barrer) but a much higher H_2/CH_4 selectivity (28.5) than CTB1-DMN (13.5). After being aged for 60 days, H_2 permeability was almost cut down to half of the initial values, while H_2/CH_4 selectivity was significantly improved. Pinnau and co-workers [55] synthesized a carboxyl-functionalized PIM-PI homopolymer. Compared to the nonfunctionalized membranes, the presence of the -COOH group promoted the formation of interchain hydrogen bonding and charge transfer complex, which led to a tighter and more size-selective structure. for the 6FDA-TrMCA membrane. With a feed condition of 2 atm and 35 °C, the resultant PIM-PI membranes showed an H_2 permeability of 193 Barrer and an H_2/CH_4 selectivity of 45.

Similar to PIMs, thermally rearranged (TR) polymers are also microporous materials with high free volume and large surface area [24]. First reported by Park et al. in 2007 [60], TR polymers are normally obtained from functionalized PIs and polyamides (PAs) which can be converted to heteroaromatic polymers (e.g., polybenzoxazoles (PBO)) after thermal rearrangement at a temperature between 350 °C and 450 °C [61, 62]. Luo et al. [56] reported PBO-based TR polymers which stemmed from PI and PA precursors

with the addition of triptycene. Two thermal processes, thermal rearrangement (TR) and thermal cyclodehydration (TC), were applied. Increased *FFV* and induced outstanding microporosity were observed owing to the introduction of triptycene, thus guaranteeing simultaneously charming permeability and selectivity of the membranes. Particularly, the membranes undergoing thermally rearrangement at 450 °C had an H_2 permeability of 810 Barrer and an H_2/CH_4 selectivity of 200 at 35 °C and 11.15 bar. Later on, TR-PBO with different triptycene concentrations and ortho-positioned functional groups (poly(o-hydroxyimide) and poly(o-acetateimide)) were successfully prepared and it is found that they initiated a positive influence on gas separation for disruption of chain packing and induced internal free volume [57]. Under optimized conditions, an ultrahigh H_2/CH_4 selectivity (203 and 125) with a promising H_2 permeability (810 Barrer and 1123 Barrer) could be obtained for TPBO and TPBO-Ac membranes. However, different from PIMs, TR polymers are more brittle and fragile after thermal treatment.

Other polymers with high porosity were also investigated for preparation of H_2/CH_4 separation membranes. For instance, by carrying out polymerization in a confined space, conjugated microporous polymers (CMPs) could react with commercial polysulfone (PSF) at a liquid-liquid interface, forming CMP@PSF membranes with outstanding H_2 sieving properties [58]. The preparation process of the high-performance CMP@PSF membrane is illustrated in **Figure 7a.** The resultant membranes showed an H_2 permeability of 4924 Barrer with an ideal H_2/CH_4 selectivity of 126.3, which is far above the 2015 upper bound. Mancilla et al. [59] synthesized a series of poly(oxindolylidene arylene)s (POXINARs) by polymerizing isatines and several aromatic hydrocarbons at room temperature. Thereinto, membranes made from isatin and 9,9-dimethyl-9H-fluorene (2aD) showed an H_2 permeability of 170 Barrer and an H_2/CH_4 selectivity of 77, which approaches the 2008 upper bound but is less attractive compared to the CMP@PSF membranes.

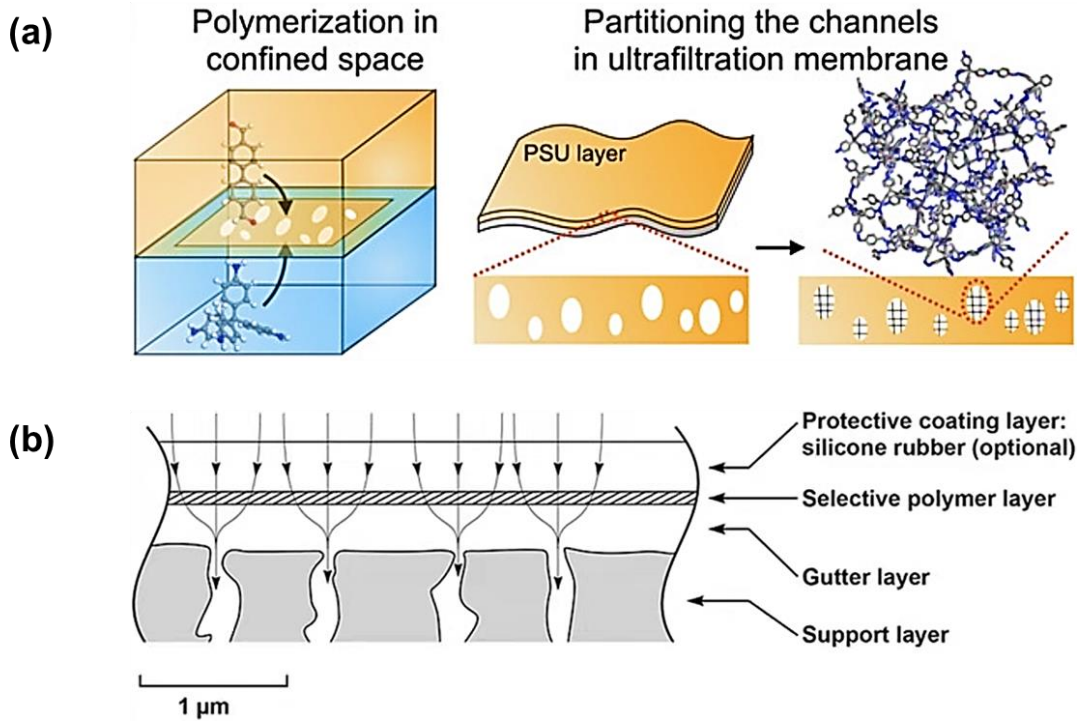

Figure 7. (a) Schematic illustration of the preparation of high-performance CMP@PSF membranes. Reproduced from [38]. (b) Structure of a multi-layer composite membrane. Reproduced from [51].

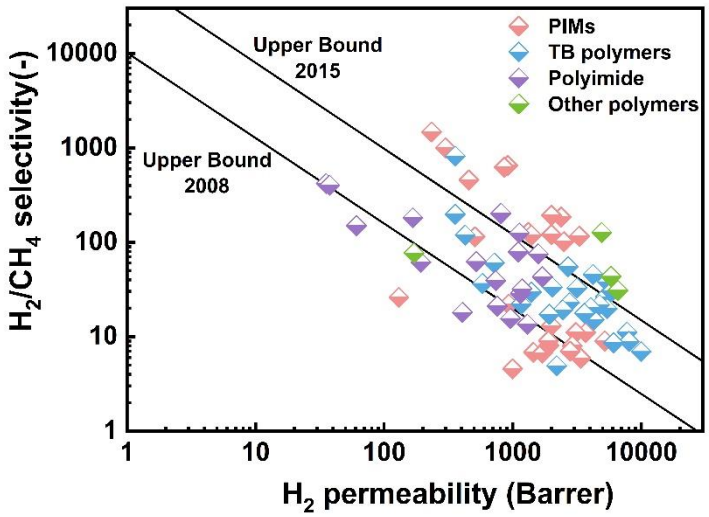

Figure 8. Separation performance of polymeric membranes for H_2/CH_4 gas pair.

Advances in H_2/CH_4 separation performances of polymeric membranes were summarized in **Figure 8**. As can be seen from **Figure 8**, for most polymeric membranes, the H_2/CH_4 separation performances are close to or slightly higher than the 2015 upper bound, demonstrating that microporous polymers, primarily represented by PIMs, TB

polymers and PIs, are promising candidates to prepare membranes for H_2/CH_4 separation. Interestingly, for some PIMs, the aged membranes present higher selectivity compared to fresh samples. Therefore, future research may carry out on developing methods to control the extent of physical aging of membranes to approach better H_2/CH_4 separation performance. In addition, highly rigid polymer chains result in high microporosity and free volume, but it presents weak mechanical properties [63, 64]. Therefore, how to balance the mechanical strength and gas separation performance of those highly porous membranes is of vital significance.

Besides self-standing membranes with a thickness of normally over 50 μm, thin-film composite (TFC) membranes with a selective layer thinner than 1 μm are more practical in industrial applications. **Table 5** summarized the progress of TFC membranes with a polymeric selective layer for H_2/CH_4 separation in recent years.

Table 5. H_2/CH_4 separation performances of TFC membranes with polymeric selective layer.

Membrane materials	**P_{Feed} (bar)**	**T (°C)**	**P_{H_2} (GPU)**	**α_{H_2/CH_4} (-)**	**Ref**
Poly(PFMMD)	3.45	22	1140	57	[65]
Poly(PFMMD-co-PFMD) 1	3.45	22	1490	80	
Poly(PFMMD-co-PFMD) 2	3.45	22	1100	157	
Poly(PFMMD-co-PFMD) 3	3.45	22	1200	162	
Poly(PFMMD-co-CTFE) 1	3.45	22	633	144	
Poly(PFMMD-co-CTFE) 2	3.45	22	457	194	
Poly(PFMMD-co-CTFE) 3	3.45	22	254	284	
PBDI	1	100	71.7	47.5	[66]
Teflon AF 2400	-	-	1050	4.6	[67]
Hyflon AD 60	-	-	1700	23	
Cytop	-	-	290	48	
Copolymer II	-	-	820	48	
Copolymer III	-	-	700	72	
Copolymer IV	-	-	700	130	

PTI	-	250	1500	60	[68]
6FDA-ODA	3	25	190	100	[69]
PDMS/PEI	1	25	4.3	96	[70]
P(DVB-co-ZnTPC)-80/PTMSP	5.07	25	45.0	550	[71]
P(DVB-co-ZnTPC)-40/PTMSP	5.07	25	68.3	210	
PTMSP	5.07	25	674	1.0	
ZnTPP/PTMSP	5.07	25	540	2.0	
P(ZnTPC)-20/PTMSP	5.07	25	272	133	
P(ZnTPC)-40/PTMSP	5.07	25	139	143	
P(ZnTPC)-80/PTMSP	5.07	25	76.9	402	

Surprisingly, some commercially available perfluoro polymers present good H_2/CH_4 separation performances. For instance, by coating Hyflon AD 60 onto a proper porous substrate, an H_2 permeance of up to 1700 GPU with an H_2/CH_4 selectivity of 23 were obtained [67]. The classic structure of a multi-layer composite membrane can be seen in **Figure 7b**. To improve the processability of the membranes, Okamoto et al. [67] synthesized several kinds of perfluorodioxolane monomers with a high glass transition temperature (T_g). These monomers can be polymerized in solution so that they can mass-produce membranes. Under optimized conditions, the synthesized copolymers simultaneously performed outstanding H_2 permeance (700 GPU) and H_2/CH_4 selectivity (130).

Fang et al. [65] applied a copolymerization method to enhance the gas separation performance of perfluoro(2-methylene-4-methyl-1,3-dioxolane) (PFMMD) membranes. They employed tetrafluoroethylene to increase gas selectivity and perfluorodioxole rings to maintain the copolymer stays at an amorphous state. Two new monomers, perfluoro-(2-methylene1,3-dioxolane) (PFMD) and chlorotrifluoroethylene (CTFE), have been developed to enhance membrane selectivity. When copolymerized with PFMMD, copolymers showed a tunable size-sieving selectivity with variation in the number of monomers. Among those polymers, the most selective one possessed an H_2/CH_4 selectivity of 284 and an H_2 permeance of 254 GPU.

Shan et al. [66] reported thin poly(p-phenylene benzobisimidazole) (PBDI) membranes prepared by interfacial polymerization (IP). The effects of reacting duration, feed pressure and operating temperature on separation performance were investigated. The various thickness induced by different reacting duration had a distinct influence on H_2 permeance and a subtle impact on H_2/CH_4 selectivity. And the separation performance improved with rising temperature owing to an activated diffusion dominated gas transport but slightly degenerated as feed pressure increased. As-prepared membranes owned good H_2/CH_4 separation performance ($P(H_2)$ =71.7 GPU, $\alpha(H_2/CH_4)$ =47.5) at 1 bar, 100 °C, but not as promising as the fluoropolymers.

Villalobos et al. [68] reported a new method to synthesize poly(triazine imide) (PTI). They successfully synthesized PTI platelets with 70% yield with respect to the precursor in a fairly safe ambient pressure condition. The triangular pores of PTI were observed by electron microscopy and these nanopores had a size-sieving effect on H_2/CH_4 gas pair. As-prepared PTI nanosheet-based membranes possessed high-temperature H_2 sieving property, and demonstrated an H_2 permeance up to 1500 GPU, with an H_2/CH_4 selectivity reaching 60 at 250 °C.

Lee and co-workers [69] reported a water-casting strategy to develop TFC membranes. In this work, 6FDA and 4,4-oxydianiline (ODA) are chosen as monomers to fabricate a synthetic PI (PI-O). The membrane integrity and thickness were adjusted by controlling the dynamic viscosity at different polymer concentrations. The resultant water-cast TFC membrane consisting of a ~30 nm selective layer exhibited a high H_2 permeance (190 GPU) and an H_2/CH_4 selectivity (100). A mixed-gas permeation test simulating steam-methane reforming from natural gas was also performed and H_2 of >99 mol% purity was obtained, indicating PI-O membrane's great potential for practical application.

Boscher et al [71] developed a plasma-enhanced chemical vapor deposition (iPECVD) approach for H_2 separation membrane preparation. Zinc(II) meso-tetraphenylchlorin (ZnTPC) was chosen as a building block and crosslinked with divinylbenzene (DVB).

The as-deposited P(ZnTPC) and P(DVB-co-ZnTPC) selective layers were supported on poly(1-trimethylsilyl-1-propyne) (PTMSP) support layer. When copolymerized with DVB, ZnTPC could form a highly porous selective layer, which possessed an improved H_2/CH_4 selectivity of 550.

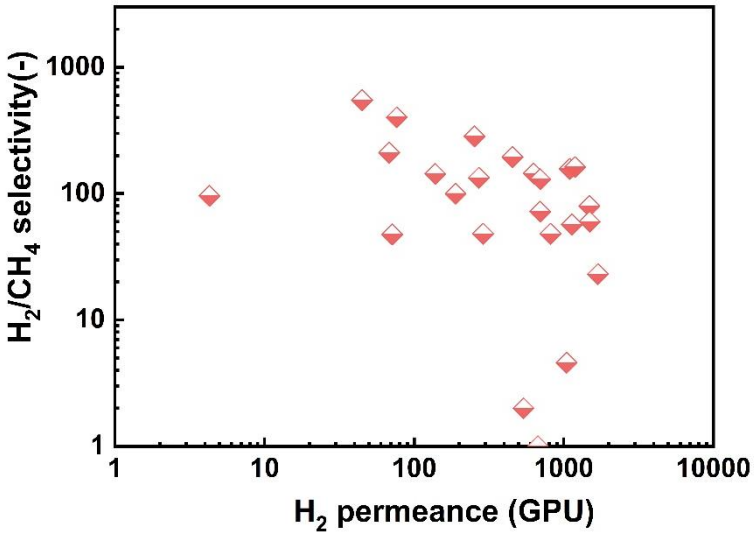

Figure 9. H_2/CH_4 separation performance of TFC polymeric membranes.

Figure 9 summarizes the progress of TFC membranes for H_2/CH_4 separation. For many membranes, an H_2 permeance of over 1000 GPU, coupled with an H_2/CH_4 selectivity of over 100 have already been obtained. To further improve the competitive capacity of polymeric membranes for H_2/CH_4 separation, further improve H_2 permeance, as well as enhance chemical and thermal stability, plasticization resistance can be a few possible directions.

4. Advances in MMMs for H_2/CH_4 separation

MMMs are composed of a continuous polymer matrix containing dispersed nano-sized inorganic particles that can combine the selectivity of the inorganic membranes with the low cost and ease of fabrication of polymer membranes [72]. Solution casting and controlled solvent evaporation are normally used to prepare MMMs [73]. Many aspects must be considered to find out an appropriate polymer/filler pair for a successful MMM,

such as size and concentration of the particle, polymer chain rigidification, the adhesion between two phases, the viscosity of particle-contained dope, and the stress of particle dispersion in the solvent [74]. Up to now, a large number of polymers have been employed as polymeric matrixes, such as polycarbonates (PC), cellulose acetate (CA), PIs, polyetherimide (PEI), PSF, poly(dimethylsiloxane) (PDMS), block copolymers [75-77].

Ideal fillers should have several properties such as (1) excellent stability under working environments, (2) high compatibility with polymeric phase, (3) improved separation performances, (4) nanosized morphology, and (5) uniform dispersity in polymer phase [74, 78]. Generally, both porous and nonporous nanofillers are applied in MMMs (as shown in **Figure 10**), and porous nanofillers are more commonly used. So far, porous materials include zeolites, covalent organic frameworks (COFs), metal-organic frameworks (MOFs), etc., and nonporous particles consist of fumed silica, carbon nanotubes (CNTs), graphene and graphene oxide (GO), etc. There have existed tons of work focusing on fillers selection and MMMs preparation, which can be found in several reviews [79-82]. The current work will mainly focus on MMMs for H_2/CH_4 separation.

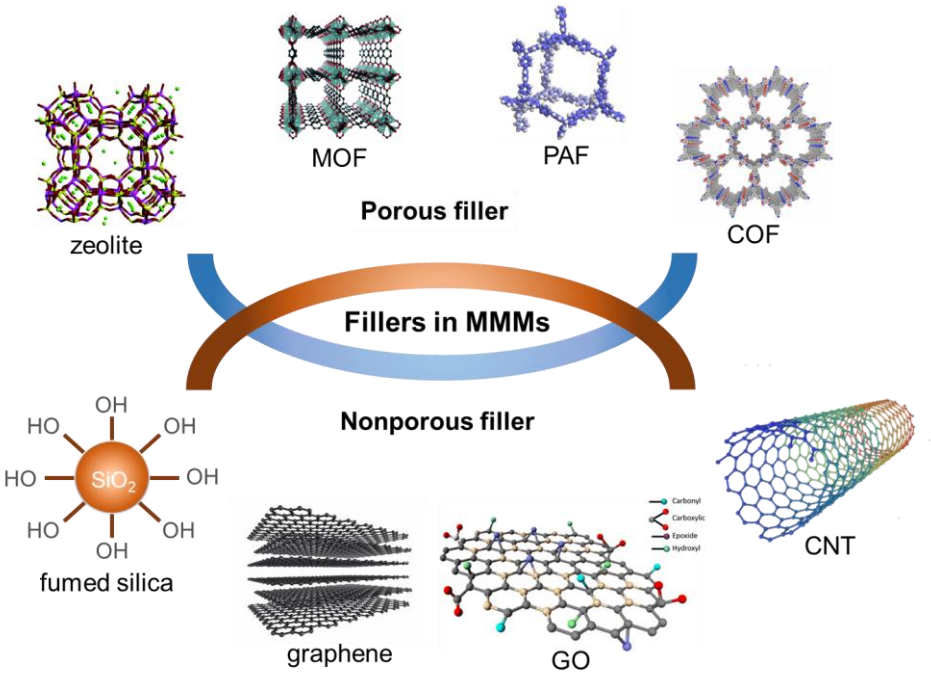

Figure 10. Commonly used porous fillers and non-porous fillers in MMMs.

4.1 Porous nanofillers

As a class of aluminosilicate crystals, zeolites have a molecular sieving nature with pore size varying from 4 Å to 12 Å and frameworks formed by interconnecting channels [83] and have been employed in making MMMs for gas separations. Si and Al are the main building block of zeolite nanocrystals, the morphology of which can be tuned by adjusting the Si/Al ratio via the change of pore sizes distribution and adsorption capacities [83, 84]. MOFs are another big family employed in MMMs fabrication [76]. MOFs are hybrid materials composed of organic bridging ligands and inorganic metal nods [83, 85]. Some types of MOFs can separate molecules with high flux and high selectivity by molecular sieving and preferential adsorption mechanisms [86]. Their ultrahigh porosity, enormous internal surface areas as well as the remarkable variability of both the organic and inorganic parts, equip MOFs with huge potential for their applications in clean energy, especially in H_2/CH_4 separation [85, 87]. Similar to MOF, COFs have also been applied in the fabrication of MMMs. **Table 6** summarizes the progress of MMMs with porous nanofillers for H_2/CH_4 separation.

Table 6. H_2/CH_4 separation performances of MMMs with porous fillers

Membrane materials	**P_{Feed} (bar)**	**T (°C)**	**P_{H_2} (Barrer)**	**α_{H_2/CH_4} (-)**	**Ref**
TBDA2-6FDA	1	35	390	48	[88]
TBDA2-6FDA/7%ZIF-8	1	35	790	38	
TBDA2-6FDA/20%ZIF-8	1	35	1443	34	
TBDA2-6FDA/30%ZIF-8	1	35	2585	28	
TBDA2-6FDA/7%ZIF-8 coated with PD	1	35	600	40	
TBDA2-6FDA/20%ZIF-8 coated with PD	1	35	1156	39	
TBDA2-6FDA/30%ZIF-8 coated with PD	1	35	1858	36	

TR (from HPI)	1	35	417	22.7	[89]
TR/10%ZIF8	1	35	362	59.8	
TR/20%ZIF8	1	35	1206	25.7	
APBO/30%ZIF8	1	35	212	55.4	[90]
APBO/35%ZIF8	1	35	386	44.3	
6FDA-DAM	4	25	498.3	18.7	[91]
6FDA-DAM/10%Z67@Z8 (L)	4	25	662.1	22.9	
6FDA-DAM/20%Z67@Z8 (L)	4	25	1154.1	21.4	
6FDA-DAM/10%Z67@Z8 (S)	4	25	615	25	
6FDA-DAM/20%Z67@Z8 (S)	4	25	967.8	22.4	
6FDA-BI	4	35	33.4	278.2	[92]
6FDA-BI/20% ZIF-8	4	35	78.5	223.9	
6FDA-BI/20% ZIF-8 (0.004 Zn^{2+})	4	35	88.2	233.4	
6FDA-BI/20% ZIF-8 (0.007 Zn^{2+})	4	35	110.1	225.2	
6FDA-BI/20% ZIF-8 (0.01 Zn^{2+})	4	35	72.3	318.3	
6FDA-DAM	4	30	21.4	33.97	[93]
6FDA-DAM/10%ZIF-11	4	30	106.7	30.49	
6FDA-DAM/20%ZIF-11	4	30	272.5	32.83	
6FDA-DAM/30%ZIF-11	4	30	76.8	32	
PEI-Ultem® 1000	4	35	8.99	183.46	[94]
PEI-Ultem® 1000/10%ZIF-12	4	35	16.56	262.86	
PEI-Ultem® 1000/20%ZIF-12	4	35	24.74	284.37	
PEI-Ultem® 1000/30%ZIF-12	4	35	39.77	331.41	
Dense PI	4.06	35	4.25	108.9	[95]
Self-consistent PI	2.03	35	128.7	31.4	
Dense PI/5%ZIF-302	4.06	35	11.22	110.2	
Self-consistent PI/5%ZIF-302	2.03	35	156.4	51.0	
6FDA-TP	9.93	35	59	113	[96]
6FDA-TP/10%ZIF-90	9.93	35	61	99	
6FDA-TP/20%ZIF-90	9.93	35	77	103	
6FDA-TP/40%ZIF-90	9.93	35	131	103	
6FDA-TP/50%ZIF-90	9.93	35	179	101	

PEI	2.03	35	856.1	45.3	[97]
PEI/5% nZIF-7	2.03	35	207.0	41.4	
PEI/5%PSM-nZIF-7	2.03	35	2020.9	18.7	
Tolidine-DMM/20%ZIF-L-Zn	2	25	897.5	23	[98]
Tolidine-DMM/20%ZIF-L-Co	2	25	1235.5	25	
Tolidine-DMM/20%ZIF-L-Co	2	60	1985.9	10	
Matrimid 5218®	-	-	11.6	82.85	[99]
Matrimid 5218®/15% UiO-66	-	-	64.4	153.3	
Matrimid 5218®/15% ZIF-8	-	-	27.1	123.2	
COOH-PI (Durene-DABA-6FDA)	4	25	538	23.1	[100]
COOH-PI/5%NH_2-UiO-66	4	25	848	25.2	
COOH-PI/10%NH_2-UiO-66	4	25	930	28.2	
COOH-PI/20%NH_2-UiO-66	4	25	1180	27.2	
6FDD	3	35	180	32.7	[101]
6FDD/20% UiO-66-NH_2	3	35	309	31.5	
6FDD/40% UiO-66-NH_2	3	35	992	32.0	
6FDD/55% UiO-66-NH_2	3	35	2934	34.4	
6FDD/60% UiO-66-NH_2	3	35	5389	4.3	
6FDD/20% UiO-66-$(OH)_2$	3	35	310	38.6	[102]
6FDD/40% UiO-66-$(OH)_2$	3	35	497	37	
6FDD/50% UiO-66-$(OH)_2$	3	35	907	45	
PEI/30%M2(dobdc)	1	25	20	8	[103]
6FDA-Durene-DABA	3	25	538	23.4	[104]
6FDA-Durene-DABA/2%CBMNs	3	25	410	41	
6FDA-Durene-DABA/5% CBMNs	3	25	288	41.1	
6FDA-Durene-DABA/15% CBMNs	3	25	140	46	
6FDA-DAM *	2	35	480	16.5	[105]
6FDA-DAM/8% MSS *	2	35	686	20.0	

6FDA-DAM/8% Mg-MSS *	2	35	794	21.8	
6FDA-DAM/8% HZS *	2	35	541	25.4	
6FDA:DAM	2	35	473	15.7	
6FDA-DAM/8% MSS	2	35	676	19.8	
6FDA-DAM/16% MSS	2	35	970	19.8	
Uncoated PDMS-neat	2	25	22.72	14.66	[106]
Uncoated PDMS- P84/0.5%ZTC	2	25	35.45	18.26	
Uncoated PDMS- P84/1%ZTC	2	25	47.44	21.02	
Uncoated PDMS- P84/1.5%ZTC	2	25	34.92	15.21	
Coated PDMS-neat	2	25	8.95	41.81	
Coated PDMS-P84/0.5%ZTC	2	25	13.15	37.29	
Coated PDMS-P84/1%ZTC	2	25	31.09	45.09	
Coated PDMS-P84/1.5%ZTC	2	25	29.10	45.09	
Neat PSF	5	25	21.36	7.77	[107]
uncoated PSF/0.4%ZTC	5	25	19.80	28.88	
coated PSF/0.4%ZTC	5	25	13.63	70.07	
DAM	2	25	103.8	14.1	[108]
DAM/5% PAF-1	2	25	434.2	31.6	
DAM/10% PAF-1	2	25	593.4	19.3	
DAM/5% cPAF	2	25	112.5	30.4	
DAM/10% cPAF	2	25	338.9	15.6	
TPIM-2	2	25±1	1651	16	[109]
TPIM-2/5% PAF-1	2	25±1	2907	24.2	
TPIM-2/10% PAF-1	2	25±1	4886	18.8	
Aged TPIM-2	2	25±1	1175	35.2	
Aged TPIM-2/5% PAF-1	2	25±1	1335	77.8	
Aged TPIM-2/10% PAF-1	2	25±1	2440	62.6	
6FDD	3	35	192.1	48.6	[110]
6FDD/2% PGF-1	3	35	226.6	47.7	
6FDD/4% PGF-1	3	35	233.7	46.7	
6FDD/6% PGF-1	3	35	421.44	49.7	
6FDD/8% PGF-1	3	35	262.1	47.6	

Matrimid/10% silicalite	3.03	35	28.3	94.3	[111]
Matrimid/10%SAPO-34	3.03	35	25.2	105	
Matrimid/10%ZIF-8	3.03	35	46.3	102.9	
PI/50%ZIF-7	2	100	997 GPU	135.3	[112]
PI/50%ZIF-7 *	2	100	897 GPU	128.4	

* Gas permeation results obtained via mixed gas permeation tests.

As a sub-family of MOFs, zeolitic imidazolate frameworks (ZIFs) are a favorable class of porous materials that have the advantages of outstanding stability, flexible structure like zeolites, high porosity and organic functionality comparable to that of polymers [113]. Thus, they are universally attractive as fillers for MMMs. Recently, amounts of ZIF/polymer MMMs with enhanced separation performance have been reported [89, 93, 114, 115]. ZIF-8 is resistant to solvent and has a teeny crystallographic pore size between the kinetic diameters of H_2 (0.29 nm) and CH_4 (0.38 nm), therefore, it has been widely studied for H_2/CH_4 separation.

By choosing a TB-based microporous PI as polymeric matrix and a polydopamine (PD) coating layer with ZIF-8 particles as fillers, Wang et al. [88] successfully fabricated MMMs for H_2/CH_4 separation. The modification of ZIF-8 fillers effectively improved the compatibility between ZIF particles and polymeric matrix. The resulting membrane show an excellent H_2 permeability of 1858 Barrer and an high selectivity of 35.7 with a ZIF-8 loading of 30 *wt.*%.

In another study, TR polymers were used as the polymeric phase instead of PIs to hold ZIF-8 particles [89]. Similar to TR polymers discussed in section 3, the TR process improved gas separation properties due to induced regulable pore size and hour-glass shape pore distributions. Additionally, the TR process also contributed to vanishing interfacial voids between the polymer matrix and ZIF particles which usually occur in most MMMs. Under optimized conditions, the TR ZIF-8 MMMs outperform the 2008 upper bound with an H_2 permeability of 1206 Barrer and an H_2/CH_4 selectivity of 25.7. Japip et al. [90] developed MMMs based on TR polymer and ZIF-8 in a similar way.

They prepared amide-derived PBO (APBO) using poly(hydroxyamide) (PHA) by a TR process with incorporated ZIF-8 particles. The presence of ZIF-8 particles also resulted in a decrease in TR temperature, which possibly owed to lower inter-chain interactions derived from the introduction of ZIF-8 particles. APBO-ZIF-8 membrane with 35 *wt.*% ZIF-8 loading showed an H_2 permeability of 386 Barrer and an H_2/CH_4 selectivity of 44.3 at 1 bar and 35 °C.

Deng et al. [98] attempted to develop MMMs with 2D ZIF-8 for H_2/CH_4 separation. ZIF-L-Zn and ZIF-L-Co were incorporated into TB-based polymer (Tolidine-DMM) respectively. Such nano-leaves were greatly compatible with the polymer phase and thereby desirable good dispersion was obtained. Meanwhile, the 2D structure of leaf ZIF endowed H_2 with a special transport pathway, enhancing its permeability up to 4 times. The ZIF-L-Co performed better in promoting gas permeabilities than ZIF-L-Zn, with 1235.5 Barrer at 20 *wt.*% loading at room temperature and up to 1985.9 Barrer at 60 °C, which exceeded the 2008 upper bound of H_2/CH_4 separation.

Other than changing ZIF-8's morphology, Yuan et al. [91] synthesized ZIF-67@ZIF-8 core-shell nanoparticles (ZIF-67 acting as the core and ZIF-8 as the shell) by seed-mediated growth and incorporated them in varying ratios into 6FDA-DAM matrix. These core-shell particles exhibited superior thermal stability, gas uptake and specific surface area than pristine MOFs. The influence of ZIF-67@ZIF-8 crystal loading on gas separation performance was also explored. And the ZIF-67@ZIF-8 MMMs showed greatly improved permeability and selectivity than pure PI membranes, Z67@Z8(L) with thicker shell size was more selective, performing an H_2 permeability of 1154.1 Barrer together with an H_2/CH_4 selectivity of 21.4 with a MOF loading of 20 *wt.*% at 4 bar and 25 °C.

To reduce the defective voids in MMMs, Li and co-workers [92] systematically tuned the polymer-filler interfacial interaction by a Zn^{2+} post-modification method. Imidazole-containing PIs were used as the polymer matrix, which could create more positive interaction with the imidazole linker in ZIF-8, thus leading to better interfacial

compatibility. Compared to the pristine PI membranes, MMMs with 20 *wt.*% ZIF-8 loading resulted in a 2.2-fold increase in H_2 permeability (78.5 Barrer) with an exceptional H_2/CH_4 selectivity of 224. After treatment of Zn^{2+} concentration at 0.007 g/mL, an enhancement in H_2/CH_4 separation performance was observed with a selectivity of 318.3 and H_2 permeability was ~72.3 Barrer. As-prepared all Zn^{2+} modified membranes exceeded the 2008 Robeson upper bound.

Al-Maythalony et al. [97] developed a series of PEI-based MMMs by combing ZIF-7 or ZIF-7 after post-synthetic modification (PSM) by linker exchange of benzimidazolate to benzotriazolate. Supreme improvement of gas separation properties of PSM-nZIF-7/PEI membrane than pure PEI membrane and nZIF-7/PEI membrane was observed: an H_2 permeability of 2020.9 Barrer and an H_2/CH_4 selectivity of 18.7. Ma et al. [112] reported ZIF-7@PI MMMs where ZIF-7 sheets dominated the molecular pathway for H_2 permeation. The ZIF-7@PI membranes blocked CH_4 molecules and showed an excellent H_2/CH_4 separation factor of 135.3 and a high H_2 permeance of 997 GPU.

Boroglu et al. [93] developed MMMs for H_2/CH_4 separation with 6FDA-DAM and ZIF-11 particles. Pristine PI presented an H_2 permeability of 21.4 Barrer, adding 20 *wt.*% ZIF-11 into PI resulted in an H_2 permeability increment to 272.5 Barrer at 4 bar and 30 ℃, while a further increase of the ZIF-11 content in PI to 30% resulted in a decline of H_2 permeability, which is only 76.8 Barrer. The good part for these MMMs is that despite the ZIFs content varies a lot, the H_2/CH_4 selectivity stayed almost unchanged (~32). Later, ZIF-12 crystals were synthesized and blended with a commercial PEI (PEI-Ultem® 1000) to form MMMs [94]. Due to the uniform distribution of ZIF-12 particles in the PEI matrix, both H_2 permeability and H_2/CH_4 selectivity were simultaneously improved. MMMs loading 30 *wt.*% ZIF-12 possessed a fairly good H_2 permeability (39.77 Barrer) and a remarkable H_2/CH_4 selectivity (331.41), thus approaching the 2008 Robeson upper bound.

In another work, Ghanem et al. [95] employed ZIF-302 to fabricate MMMs with PI

resin as the matrix. Dense PI (d-PI)/ZIF-302 and self-consistent PI (s-PI)/ZIF-302 were prepared via different synthesis methods. Both MMMs displayed an increase in gas permeability and s-PI/ZIF-302 behaved particularly well for an H_2 permeability of 156.4 coupled with an H_2/CH_4 selectivity of 51.

Zhang and co-workers developed MMMs with triptycene-based PI and ZIF-90 [96]. Due to the interaction between organic ligands in ZIF-90 with imide moieties in PI, ZIF-90 particles dispersed well without aggregation. The presence of ZIF-90 crystals also assisted H_2 diffusion due to the highly microporous structure of ZIF-90. The resulting MMMs revealed significantly enhanced H_2 permeability with negligible selectivity loss. An H_2 permeability of 179 Barrer with an H_2/CH_4 selectivity of 101 were achieved for MMMs with 50 *wt.*% ZIF-90 loading, the permeability was 3 times higher than the pristine PI membrane.

UiO-66, which is typically built from zirconium oxide ($Zr_6O_4(OH)_4$) nodes linked by 1,4-benzendicarboxylate as a bridging ligand, was also considered a promising nanofiller in membranes due to its ultrafine thermal, chemical, and mechanical stabilities as well as its high surface area [83, 116].

Aiming at exploring the potential of separating the gas mixture produced from a methane reforming process, MMMs were prepared with Matrimid 5218® as a polymer matrix, ZIF-8 and UiO-66 as nanofillers [99]. In the single gas permeation test, MMMs with UiO-66 as nanofillers exhibited an H_2 permeability of 64.4 Barrer and an H_2/CH_4 selectivity of 153.3. On the other hand, MMMs with ZIF-8 as nanofiller showed an H_2 permeability of 27.1 Barrer and an H_2/CH_4 selectivity of 123.2. For both cases, H_2 permeability and H_2/CH_4 selectivity were significantly improved. However, UiO-66 was more effective in promoting H_2 permeability and hindering CH_4 transport, thus resulting in higher values in both H_2 permeability and H_2/CH_4 selectivity.

Wang et al. [100] utilized a low-temperature cross-linking strategy to enhance the stability of MMMs formed by carboxylic acid-functionalized PI (COOH-PI) and amine

group-functionalized UiO-66 (NH_2-UiO-66). At the same time, the effect of nanoparticle size on H_2/CH_4 separation performances was also investigated. It was found that the functionality and the particle size of MOFs played an important role in H_2/CH_4 separation performance. Nanoparticles with a larger size led to a smaller surface area and thus a weaker interfacial interaction. However, if the MOF particles were too small, the induced strong interfacial interaction and increased interface rigidity of polymers would significantly reduce H_2 permeability (as shown in **Figure 11**). In addition, increasing the nanoparticle content in MMMs leads to completely different trends. Increasing the content of 10 nm-particles in the MMMs resulted in an evident decline in H_2/CH_4 selectivity and only a slight improvement in H_2 permeability. On the other hand, if the particle size is over 30 nm, then increasing nanofiller content in the MMMs would result in a significant improvement in H_2 permeability with almost constant H_2/CH_4 selectivity. At 4 bar and 25 °C, an H_2 permeability of 1180 Barrer and an H_2/CH_4 selectivity of 27.2 at 20 *wt.*% loading could be obtained.

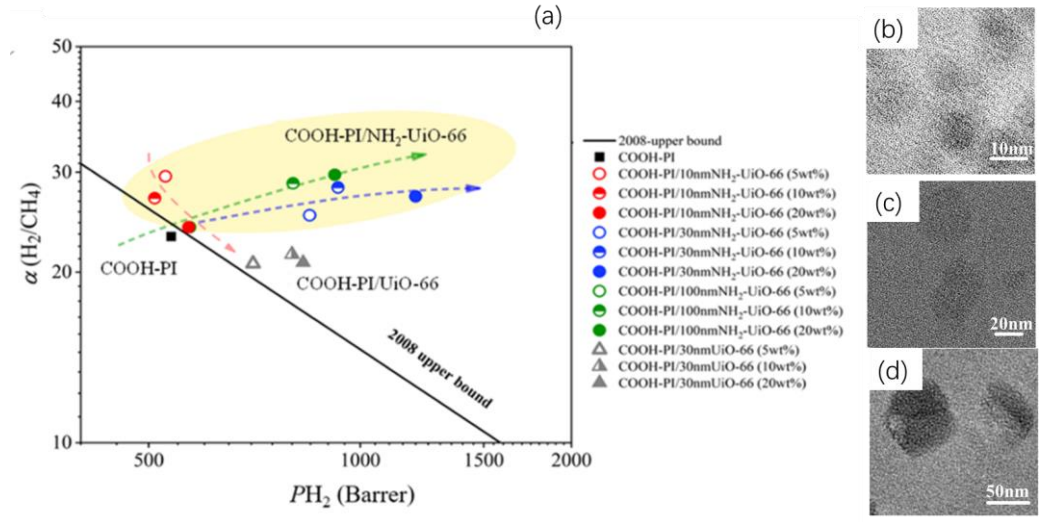

Figure 11. (a)Effect of nanoparticle size on H_2/CH_4 separation performances. Cross-sectional TEM images of (a) COOH-PI/10 nmNH_2-UiO-66 (20 *wt.*%) MMM, (b)COOH-PI/30 nm NH_2-UiO-66(20 *wt.*%) MMM, and (c) COOH-PI/100 nm NH_2-UiO-66 (20 *wt.*%) MMM. Reproduced from ref [100].

In another study, Urban et al. [101] employed UiO-66-NH_2 and carboxylic 6FDA-DAM:DABA (3:2) (6FDD) to fabricate MMMs for H_2/CH_4 separation. Up to 55 *wt.*%

of UiO-66- NH_2 was added into the PI matrix, which broke the restriction of MOFs content always in the range of 10~40 *wt.*%. MMMs with 55 *wt.*% UiO-66-NH_2 demonstrated an H_2 permeability of 2932 Barrer and an H_2/CH_4 selectivity of 34.4, considerably surpassing the current Robeson upper bounds at 3 bar and 25 ℃. Several months later, the same group incorporated UiO-66-$(OH)_2$ into carboxylic 6FDD, resulting in desirable carboxylic moieties in the polymer chains and excellent H_2/CH_4 separation performance with an H_2 permeability of 907 Barrer and an H_2/CH_4 selectivity of 32. It was estimated that the superior performance derived from favorable interactions at the boundary of hydroxy UiO-66 and carboxylic polymers via intensive hydrogen bonds, enlightening a novel synthesis strategy for improving the established membranes [102].

Smith et al. reported a new MMM fabricated by incorporating M_2(2,5-dioxido-1,4-benzenedicarboxylate) (M_2(dobdc), M=Mg/Ni) nanofillers into a PEI copolymer [103]. Defect-free membranes with up to 51 *wt.*% M_2(dobdc) loading could be fabricated under a relatively high ether content. The resultant membranes show a slightly enhanced gas separation behavior compared with neat polymer (H_2/CH_4 selectivity increased from 6.8 to 8, while H_2 permeability increased from 13 to 20 Barrer); nevertheless, this improvement would be offset by significantly declined mechanical property thus not practically promising for H_2/CH_4 separation.

Bi et al. [104] prepared Co-benzenedicarboxylate (Co-BDC) MOF nanosheets (CBMNs) which possessed a large number of metal ions on the surface and could construct more interfacial metal coordination with the polymer phase. The MOF nanosheets were used to form MMMs with carboxyl-functionalized 6FDA-Durene-DABA. Co^{2+} in the fillers interacted well with the -COOH group in the polymer, thus the MMMs had an improved solid-liquid transition and exhibited an improved H_2/CH_4 selectivity up to 41 with a slightly decreased H_2 permeability of 410 Barrer.

Zornaza et al. [105] investigated the effect of surface modification on the separation performance of MMMs that were fabricated by 6FDA-DAM polymer coupled with

ordered mesoporous silica MCM-41 spheres (MSSs), Grignard surface-functionalized MSSs (Mg-MSSs) and hollow zeolite spheres (HZSs), respectively. The membranes based on HZSs showed higher selectivity (180) but lower permeability (38.4 Barrer) compared with those based on MSSs. The $Mg(OH)_2$ nanostructure modification improved the fillers' adherence to the polymer and MMM with 8 *wt.*% Mg-MSS loading was found with the best performance with an H_2/CH_4 selectivity of 21.8 and an H_2 permeability of 794 Barrer. However, its performance still did not surpass the upper bound.

Gunawan et al. [106] incorporated different loading amounts of zeolite-templated carbon (ZTC), a unique micro-mesoporous carbon particle into P84 membranes. Compared with the neat P84 membrane, all the ZTC-filled membranes exhibited boosted H_2 permeability. And membranes with 0.5, 1.0 and 1.5 *wt.*% ZTC loading were 8.95, 13.15, 31.09 and 29.10 Barrer, respectively. Meanwhile, the membrane with 1 *wt.*% ZTC loading showed an excellent H_2/CH_4 selectivity of 45.09. Rika et al. [107] fabricated PSF-based MMMs by combing porous ZTC fillers synthesized from sucrose and zeolite-Y. The introduction of ZTC with high affinity to H_2 molecules significantly improved H_2/CH_4 selectivity (802%) compared with neat PSF (from 7.77 to 70.07).

Porous aromatic frameworks (PAFs) are porous materials having exceptionally high Langmuir surface area and better thermal and hydrothermal stabilities than MOFs. In some cases, high H_2 uptake capacity was also documented (10.7 *wt.*% at 77 K, 48 bar) [117]. Smith et al. [108] fabricated a TR-MMM based on PAF-1-containing 6FDA-HAB_5DAM_5 and it showed a 37-fold enhancement in H_2 permeability and a similar selectivity improvement. Hill and co-workers [109] prepared MMMs by incorporating PAF-1 into a phenazine-containing triptycene ladder polymer (TPIM-2), thus achieving an enhancement both in selectivity (18.8) and H_2 permeability (4886 Barrer). After physical aging, the selectivity could go up to 62.2 coupled with fairly good permeability, which resulted in the aged MMMs transcending the 2015 upper bound for H_2/CH_4 separation. Most importantly, it was found that the presence of PAFs reduced the

process of physical aging, which solved the problem that most high free volume polymers had in the past few years.

Pyrazine-fused porous graphitic frameworks (PGFs), a chemically synthesized class of graphene derivatives, have shown their potential in MMMs as nanofiller. Cacho-Bailo et al. developed a novel MMM by incorporating crystalline PGF-1 into 6FDD [110]. At 6 *wt.*% PGF-1 loading, the MMMs displayed an H_2/CH_4 selectivity of 49.7 with an H_2 permeability of 421.4 Barrer.

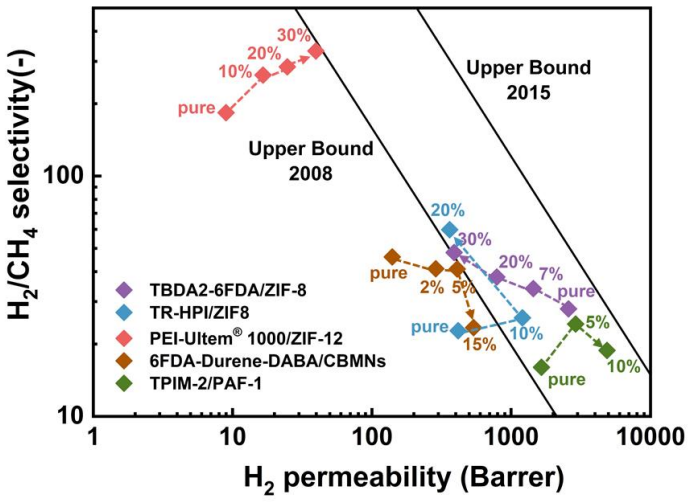

Figure 12. H_2/CH_4 separation performance of porous filler-based MMMs with different nanofiller content.

The H_2/CH_4 separation performances of MMMs with various loadings of fillers are presented in **Figure 12.** As can be seen from the figure, different trends can be obtained for MMMs with various fillers. In most cases, as the loading of fillers increases, the H_2 permeability of the MMMs witnesses a rise, and the H_2/CH_4 selectivity declines accordingly (e.g., 6FDA-Durene-DABA/CBMNs). On the other hand, it is also commonly seen that the gas permeability firstly goes up and then drops down when further increasing the nanofiller content in the MMMs (e.g., TPIM-2/PAF-1). For ideal MMMs with good compatibility between the nanofiller and polymeric phase, both high gas permeability and selectivity can be obtained when increasing the nanofiller content in the MMMs (e.g., Ultem/ZIF-12).

Figure 13 presents the H_2/CH_4 separation performances of MMMs with porous nanofillers. Although many MMMs using different porous nanofillers have been developed, almost all the membrane performances lie under the 2015 H_2/CH_4 upper bound. In addition, most MMMs present relatively high H_2 permeability and low H_2/CH_4 selectivity.

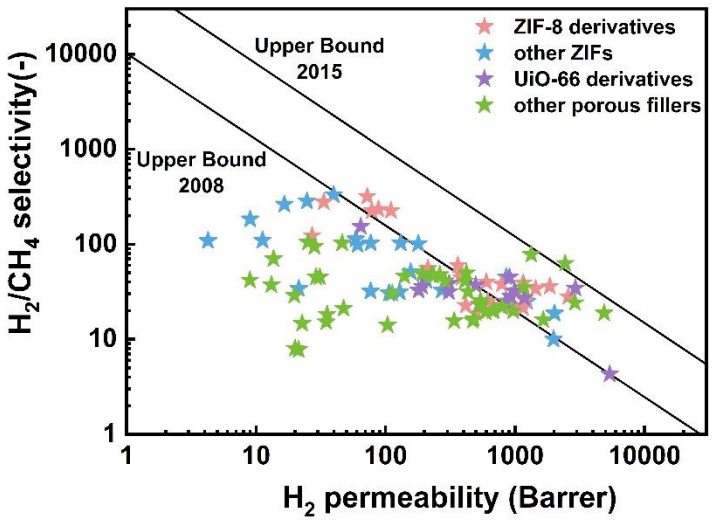

Figure 13. H_2/CH_4 separation performance of state-of-the-art porous filler-based MMMs.

To sum up, among common porous fillers, zeolites and COFs are almost not researched in terms of MMMs used for H_2/CH_4 separation, while MOFs, especially ZIFs have been widely investigated. Thereinto, ZIF-8 and UiO-66 are representatives. Other porous fillers, such as MOF nanosheets, mesoporous silica, zeolite-templated carbon, porous aromatic framework, and porous graphitic frameworks, also have been explored for their potential for H_2/CH_4 separation. Nevertheless, as can be seen from **Figure 14**, most of them behave quite mediocrely and only a few are close to or surpass the upper bound limit.

4.2 Nonporous nanofillers

Nonporous nanofillers, such as graphene, GO, CNTs and fumed silica, have been also used in the fabrication of MMM for H_2/CH_4 separation. **Table 7** lists the recent progress

for the MMMs for H_2/CH_4 separation based on various nonporous fillers.

Table 7. H_2/CH_4 separation performances of MMMs

Membrane materials	P_{Feed} (bar)	T (°C)	P_{H_2} (Barrer)	α_{H_2/CH_4} (-)	Ref
CTA	1.5	25	4.39	36.58	[118]
CTA/2.5% TNT	1.5	25	12.83	42.77	
CTA/2.5% CNT	1.5	25	15.83	38.61	
CTA/2.5% TNT@CNT	1.5	25	22.28	48.43	
PBNPI	1.96	26	4.71	6.72	[119]
PBNPI/1% MWCNT	1.96	26	4.95	6.69	
PBNPI/2.5% MWCNT	1.96	26	6.49	6.83	
PBNPI/5% MWCNT	1.96	26	6.42	5.49	
PBNPI/10% MWCNT	1.96	26	12.06	7.78	
PBNPI/15% MWCNT	1.96	26	14.31	8.04	
PES *	5	-	12.6 GPU	43.6	[120]
PES/0.5% MWCNT *	5	-	16.8 GPU	14.4	
PES/1% MWCNT *	5	-	69GPU	44.1	
PES/2% MWCNT *	5	-	59.7 GPU	22.1	
XTR (from (HAB50-DAM45-DABA5)-6FDA)	1	25	218.0	24.6	[61]
FBN-XTR (from (HAB50-DAM45-DABA5)-6FDA)	1	25	96.5	322.3	
CA	1.01	25	8.4	42	[121]
CA/0.5% $(PdOAc)_2$	1.01	25	13.5	67.5	
CA/0.75% $(PdOAc)_2$	1.01	25	13.7	68.5	
CA/1% $(PdOAc)_2$	1.01	25	11.1	37	

* hollow fiber

CNTs are composed of sp^2 carbon atoms and constructed by seamless tubes made of rolled-up graphene [80]. It has been reported that if uniform dispersion in the polymer phase can be achieved, the strong C-C bond in the graphite layer will enhance the mechanical strength of MMMs even at a low loading [122-124]. In addition, molecular

dynamics simulation indicates that the diffusion of light gases like H_2 and CH_4 in the CNTs is faster than through other porous materials because of their smooth internal surface [120, 125]. Thus both single-walled carbon nanotubes (SWCNT) and multi-walled carbon nanotubes (MWCNT) have been reported for MMMs fabrication [120, 126].

Regmi et al. fabricated MMMs using a commercial CNT and home-made titanium dioxide nanotube (TNT) with cellulose triacetate (CTA) as polymeric phase [118]. It was found that the MMMs with hybrid TNT@CNT depicted a higher H_2 permeability (22.28 Barrer) than the single filler (CNT/TNT)-based MMMs and pristine CTA membranes. Although the presence of hybrid nanofillers improved the H_2 permeability and H_2/CH_4 selectivity significantly, the overall separation performance was far below the upper bound.

By combining organic poly(bisphenol A-co-4-nitrophthalic anhydride-co-1,3-phenylene diamine) (PBNPI) with MWCNTs, MWCNTs/PBNPI nanocomposite membranes were prepared by Wey et al. through solution casting method [119]. The presence of MWCNTs greatly improved H_2 permeability threefold, MMMs with 15 *wt.*% MWCNTs loading show an improved H_2 permeability of 14.31 Barrer and an H_2/CH_4 selectivity of 8.04.

Carboxylated MWCNTs were mixed into polyethersulfone (PES) dope to fabricate hollow fiber (HF) membranes by Ghomshani et al. [120]. An H_2 permeance of 69 GPU and H_2/CH_4 selectivity of 44.1 was documented for MMMs with 1 *wt.*% MWCNTs loading, which is the best H_2/CH_4 separation performance among the tested samples. Further increasing the CNT content to 2 *wt.*% resulted in both lower H_2 permeance and H_2/CH_4 selectivity due to the presence of marcoviods between the polymer phase and CNTs.

As a 2D graphene analogue, carbon nitride nanosheets can be used as nanofillers in MMMs to improve the gas separation performance, due to their specific adsorption,

torturous gas diffusion pathways and size sieving effect. Wang et al. [61] incorporated amino-functionalized boron nitride nanosheets (FBN) into a crosslinked thermally rearranged PI (XTR) to fabricate FBN-XTR nanocomposite membranes. Compared to pristine XTR membrane, FBN-XTR membrane with 1 *wt.*% FBN exhibited exceedingly improved H_2/CH_4 separation performance. Although H_2 permeability decreased from 210 to 96.5 Barrer, H_2/CH_4 selectivity increased by more than 12 folds (from 24.1 to 322.3) at 1bar and 25 °C. Meanwhile, it was also found that the presence of FBN significantly improved both tensile strength (3 times) as well as the elongation (60%).

Sajjan et al. [121]firstly employed palladium salt (palladium acetate in this work) as a filler material. And they chose cellulose acetate (CA) as a polymeric matrix for its toughness, decent hydrophilicity, good flux, and low cost. Pristine CA was blended with various concentrations (0.5, 0.75, and 1 wt %) of palladium acetate preparing CA/$(PdOAc)_2$ blend membranes via vapor-induced phase separation (VIPS) method. Tensile strength of all blend membranes was higher than that of the pure CA membrane and 0.5% composition brought optimum chemical and mechanical properties. The optimized ratio with mechanical and chemical stabilities was found: 0.75% $(PdOAc)_2$/CA membrane displayed an H_2/CH_4 selectivity of 67.5 coupled with an H_2 permeability of 13.5 Barrer.

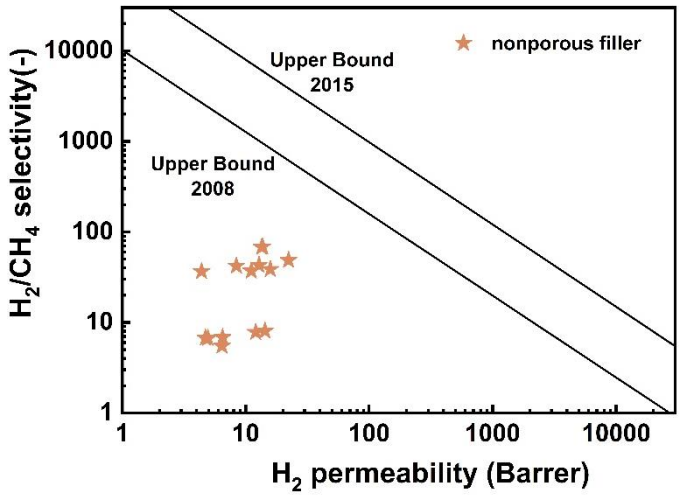

Figure 14. Separation performance of state-of-the-art nonporous filler-based mixed matrix membranes for H_2/CH_4 gas pair.

To sum up, compared with the MMMs using porous nanofillers, MMMs with non-porous nanofillers were less impressive. As shown in **Figure 14**, most H_2/CH_4 separation data for MMMs with nonporous nanofillers are far below the 2008 upper bound. One possible reason is that most MMMs with non-porous fillers started with relatively low separation polymeric membranes (e.g., CTA, CA). On the other hand, even though the presence of non-porous fillers doesn't make significant separation performances, in some cases, a small amount of the additive in the MMMs may effectively improve the mechanical properties, which can be a new opportunity for non-porous nanofillers.

5. Advances in CMS membranes for H_2/CH_4 separation

Other than polymeric membranes and MMMs, CMS membranes also have been studied for H_2 separation. CMS membranes are normally fabricated via carbonization of polymer precursors like PEI, cellulose, poly(p-phenylene oxide) (PPO) and PIs at a high temperature under a vacuum or inert atmosphere [127]. Normally, during the pyrolysis process, the polymeric chain is firstly carbonized to aromatic strands, and

then to the ordered plates, which results in a bimodal structure of ultramicropores (<0.7 nm) and micropores (0.7~2 nm) [128]. Generally, H_2 permeability of CMS membranes declines with the pyrolysis temperature increases, but the H_2/CH_4 selectivity will be increased dramatically. However, further increased pyrolysis temperature will result in collapse of micropore structure collapse and formation of impermeable sheets, which will sharply reduce both H_2 permeability and mechanical strength of membranes. The molecular sieving transport mechanism derived from their special pore size and pore distribution is of special interest for H_2/CH_4 separation. Besides, CMS membranes also have great advantages of outstanding thermal and chemical stability [129]. Generally, CMS membranes can be divided into self-standing membranes and TFC membranes.

5.1 Self-standing CMS membranes

Self-standing CMS membranes usually include flat-sheet membranes and hollow fiber membranes. The recent progress in using self-standing CMS membranes for H_2/CH_4 has been summarized in **Table 8**.

Table 8. H_2/CH_4 separation performances of self-standing CMS membranes

Membrane materials	Pyrolysis Temp (°C)	Test condition	P_{H_2} (Barrer)	α_{H_2/CH_4} (-)	Ref
P84/ZCC 1 °C/min *	800	25 °C, 2.2 bar	88.14	10.41	[130]
P84/ZCC 3 °C/min *	800	25 °C, 2.2 bar	315.84	20.71	
P84/ZCC 3 °C/min *	800	50 °C, 2.2 bar	126.91	15.55	
P84/ZCC 3 °C/min *	800	100 °C, 2.2 bar	879.91	13.45	
P84/ZCC 5 °C/min *	800	25 °C, 2.2 bar	69.03	28.86	
TB-PI	-	35 °C,	390	49	[131]

		1 bar			
TB-PI	550	35 °C, 1 bar	14600	31	
TB-PI	650	35 °C, 1 bar	6552	96	
TB-PI	800	35 °C, 1 bar	2500	200	
PABZ-6FDA-PI	550	35 °C, 1 bar	9495	96	[132]
PABZ-6FDA-PI	600	35°C 1 bar	8845	147.4	
PABZ-6FDA-PI	650	35 °C, 1 bar	4366	272.9	
PABZ-6FDA-PI	700	35 °C, 1 bar	2312	471.8	
PABZ-6FDA-PI	750	35 °C, 7 bar	1295	968	
PABZ-6FDA-PI	800	35 °C, 7 bar	460	3800	
Matrimid® *	900	35 °C, 6.89 bar	283	40350	[25]
Matrimid® *	875	35°C, 6.89 bar	463	10166	
Matrimid® *	850	35 °C, 6.89 bar	604	4516	
Matrimid® *	800	35 °C, 6.89 bar	1291	1223	
Matrimid® *	750	35 °C, 6.89 bar	1656	468	
Cellulose-based CMSMs *	850	130 °C, 2bar	150 GPU	5706	[133]

* hollow fiber

Widiastuti et al. developed a novel HF composite CMS membrane for H_2/CH_4 separation [130]. The CMS membranes were derived from P84 co-PI (**Figure 15a**) with the incorporation of zeolite composite carbon (ZCC). ZCC combines the advantages of high surface area, high microporosity, ordered pore structure and low hydrophilicity. Firstly, the effect of heating rates was investigated. It was found that when tested at 25 °C and 2.2 bar, CMS membrane obtained with a heating rate of 3 °C/min presented the highest H_2 permeability (315.84 Barrer), while CMS membrane with a 5°C/min heating rate showed the highest H_2/CH_4 selectivity (28.86). Secondly, the permeation temperature was also tested, and it was found that there was a stronger adsorption effect on H_2 than CH_4 at 50 °C and permeability was relatively low. But as the temperature increased to 100 °C, the adsorption effect was negligible. For the P84/ZCC CMS membrane carbonized with a heating rate of 3 °C/min, and tested at 100 °C and 2.2 bar, the best separation performance was observed with an H_2 permeability of 879.91 Barrer and an H_2/CH_4 selectivity of 13.45.

Wang et al. employed microporous TB-based PI as a precursor (**Figure 15b**) to prepare CMS membranes [131]. In their work, the highly contorted and rigid TB-PI backbone contributed to the membranes' good thermal stability. And the pyrolysis procedure and the soaking temperature were optimized. After thermal pyrolysis, the TB-CMS membrane witnessed a sharp rise in permeability. Along with the increasing the soaking temperature, the permeability decreased gradually and the gas selectivity increased accordingly. The obtained TB-CMS membrane with a soaking temperature of 550 °C showed an ultrahigh H_2 permeability of 14600 Barrer and an excellent H_2/CH_4 selectivity of 96 when tested at 1bar and 35 °C.

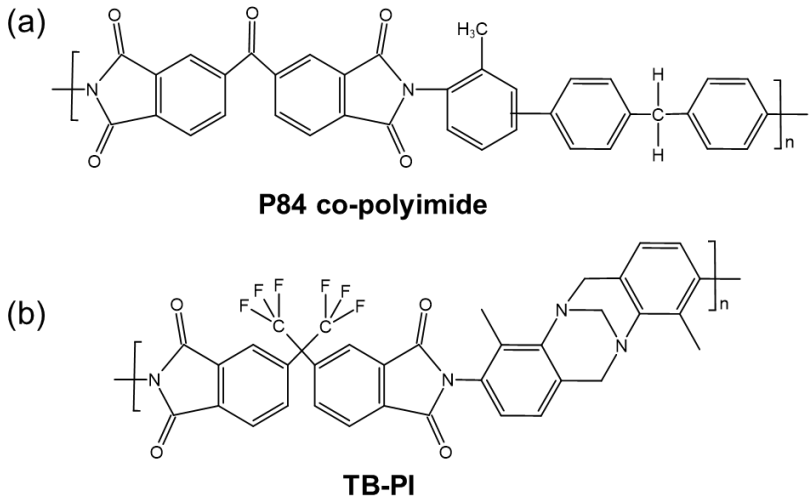

Figure 15. Chemical structure of the two highly porous PI precursors.

It is well-accepted that the chemical structure and physical properties of polymer precursors have a significant impact on the ultimate CMS membranes [132]. Jin et al. [132] explored the potential of benzimidazole-based PI (PABZ-6FDA-PI) as a precursor because of its synergistic combination of polymer chain contortion and flatness. The resulting CMS membranes displayed superior H_2/CH_4 separation performance. When carbonized at 550 °C, an H_2 permeability of up to 9495 Barrer with an H_2/CH_4 selectivity of 95 was documented at 1bar and 35 °C. Further increasing the carbonization temperature to 850 °C resulted in much lower H_2 permeability (460 Barrer) but two orders of magnitude higher H_2/CH_4 selectivity (3800), denoting this CMS membrane is a promising candidate for H_2/CH_4 separation.

Increasing sorption selectivity is a powerful tool to leverage diffusion selectivity. Koros and co-worker [25] formed a new carbon/carbon mixed-matrix (CCMM) membranes via pyrolyzing Matrimid® HF membranes at a temperature up to 900 °C. Supreme H_2/CH_4 separation performance ($P(H_2)$ = 283 Barrer, $\alpha[H_2/CH_4]$ = 40350) was displayed at 35 °C. The permeation tests indicated that such an unprecedented selectivity originated from sharply increased sorption selectivity, which may come from that the ultraselective micropores intercepting the bulkier CH_4 molecules. Further increasing the pyrolysis temperature to 900 °C resulted in an H_2/CH_4 of up to 40350,

which is among the highest values in almost all the CMS membranes.

5.2 TFC CMS membranes

Porous support is usually used to make TFC CMS membranes. Typically, a 1–5 μm thick CMS selective layer is formed by pyrolyzing a polymer precursor which is dip coated on the porous support[134]. Normally, thin self-standing membranes are fragile and are difficult to handle, and supported membranes circumvent the mechanical weakness, and thus are preferred[135]. The recent progress in using TFC CMS membranes for H_2/CH_4 has been summarized in **Table 9**.

Table 9. H_2/CH_4 separation performances of TFC CMS membranes

Membrane materials	**Pyrolysis Temp (°C)**	**Test condition**	**P_{H_2} (Barrer)**	**α_{H_2/CH_4} (-)**	**Ref**
PEI-Al_2O_3	600	25 °C, 2.02 bar	537.49	197.6	[136]
PEI-TiO_2/Al_2O_3	600	25 °C, 2.02 bar	600.7	725.9	
PEI-TiO_2/Al_2O_3 (1)	600	28 ± 2 °C, 2.02 bar	668	510	[137]
PEI-TiO_2/Al_2O_3 (2)	600	28 ± 2 °C, 2.02 bar	566	720	
PEI-TiO_2/Al_2O_3 (3)	600	28 ± 2 °C, 2.02 bar	479.1	332.9	
PEI-polished TiO_2/Al_2O_3 (4)	600	28 ± 2°C, 2.02 bar	966	200	
PEI-polished TiO_2/Al_2O_3 (5)	600	28 ± 2°C, 2.02 bar	576.5	419.0	
PEI-15%	600	28±2 °C, 2 bar	91.89 GPU	1.83	[138]
PEI-20%	600	28±2°C, 2 bar	124.91 GPU	6.72	

PEI-25%	600	28±2 °C, 2 bar	167.31 GPU	293.78	
PEI-30%	600	28±2 °C, 2 bar	48261.22 GPU	3.26	
CMSM (dry) (6)	550	35 °C, 6 bar	25.77 GPU	204.92	[139]
CMSM (humid)	550	35 °C, 6 bar	112.37 GPU	215.71	
CMSM (dry)	550	50 °C, 6 bar	56.65 GPU	249.0	
CMSM (humid)	550	50 °C, 6 bar	161.29 GPU	243.67	
CMSM (dry)	550	70 °C, 6 bar	108.25 GPU	243.01	
CMSM (humid)	550	70 °C, 6 bar	215.77 GPU	263.69	

(1) substrate cast at 10 °C
(2) substrate cast at 30 °C
(3) substrate cast at 50 °C
(4) substrate (14 μm) cast at 30 °C
(5) substrate (30 μm) cast at 30 °C
(6) CMSM was fabricated using novolac resin (13 *wt.*%), formaldehyde (2.4 *wt.*%), ethylenediamine (0.4 *wt.*%), boehmite (as a precursor of alumina 0.8 *wt.*%) mixture solved in N-methyl-2-pyrrolidone (NMP), and then coat on α-alumina tube.

Tseng et al. fabricated a supported CMS membrane by coating the selective layer on the titanium gel-modified alumina supports [136]. It was found that the TiO_2 intermediate layer controlled the interlocking pattern between the selective layer and porous Al_2O_3 support. The PEI-based CMS membrane exhibited an exceedingly improved H_2/CH_4 selectivity of 725.9 with an increased H_2 permeability of 600.7 Barrer. Later on, the same group investigated the influences of the viscosity of the PEI coating solution as well as the surface roughness of the substrate on the performance of the CMS membranes [137]. By changing the membrane casting temperature, both H_2 permeability and H_2/CH_4 selectivity can be readily tuned. The casting temperature of

30 °C was found to be optimal, and the membrane prepared under this condition displayed superior H_2/CH_4 separation performance (H_2 permeability=566.1 Barrer, selectivity=720) when tested at 28 ± 2 ℃ and 2.02 bar.

The effect of polymer conformation was also investigated. Lin et al. [138] fabricated CMS membranes from three polymer precursor conformations (dilute, semi-dilute, and concentrated) via dissolving PEI in NMP to form 15, 20, 25 and 30 *wt.*% dope solutions. It is found that the CMS membrane prepared by 30 *wt.*% PEI solution possessed the highest permeance and the lowest selectivity among all the gas pairs, suggesting the occurrence of defects after pyrolysis in the membrane. In addition, the H_2 permeance values of CMS membranes prepared by 25, 20, 15 *wt.*% PEI solution were incrementing in order, 167.31, 124.91, and 91.89 GPU, respectively. Compared to other CMS membranes, the CMS membrane prepared by 25 *wt.*% PEI solution membrane displayed a more ordered structure, thus exhibiting the highest H_2/CH_4 selectivity (293.78) and a superior H_2 permeance of 167.31 GPU.

Additionally, attention was given to the influence of ambient humidity on the transport mechanism of CMS membranes and their selectivity and purity of the permeated H_2. It was demonstrated that water adsorption was essential to enhance the performance of CMSM, especially at a high temperature. The membranes showed improved H_2 permeance from 25.77 GPU to 112.37 GPU after humidifying at 35 °C and 6 bar. Besides, an enhanced H_2 permeance of 215.77GPU and an improved H_2/CH_4 selectivity of 263.69 were obtained when tested at 70 °C and 6 bar [139]. However, the latest developed cellulose-based HF carbon membranes showed long-term stability by exposure to humidified conditions [133], which proves that hydrophilic carbon membranes can be prepared by selecting suitable precursors and controlling the carbonization procedure.

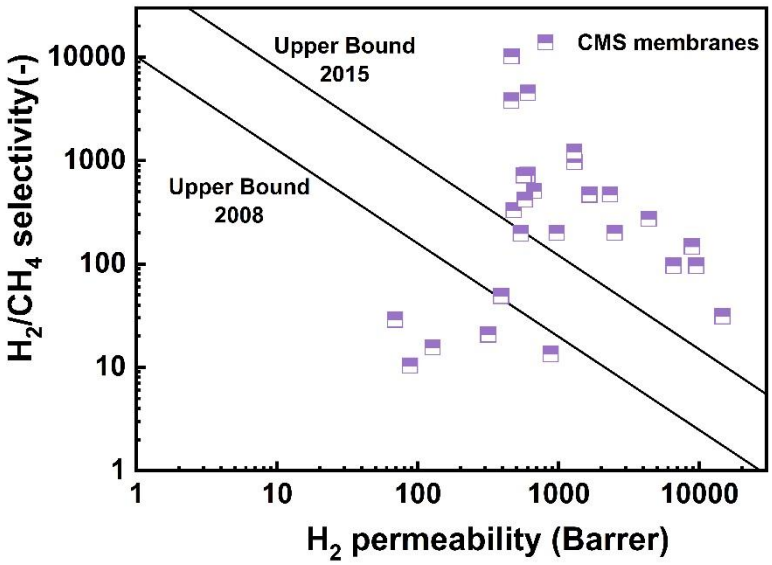

Figure 16. H_2/CH_4 separation performance of CMS membranes.

Although the number of CMS membranes is relatively less than that of polymeric membranes and MMMs, these CMS membranes behave so marvelously that most of them outperform the upper bound exceedingly (**Figure 16**). The molecular sieving effect endowed them with supreme selectivity and they also exhibit merits of thermal and chemical stability. However, such pore structure can be easily clogged, which needs pre-purification to remove vapors with a strong absorbance tendency [129]. Besides, most flat-sheet CMS membranes are brittle and fragile, which requires cautious handling, making flexible HF carbon membranes [133] can provide great potential for this application.

Figure 17 summarized H_2/CH_4 separation data for polymeric membranes, MMMs and CMS membranes. As shown in the figure, polymeric membranes display great talent in H_2/CH_4 separation. Most of the high free volume polymers exhibited H_2/CH_4 separation performances that surpass the 2008 upper bound. The representatives are microporous polymers with high free volume such as PIMs, TB polymers, and PIs.

Surprisingly, for H_2/CH_4 separations, MMMs are less attractive compared to pure polymeric membranes. Most studied MMMs show lower H_2 permeability than those

high free volume polymers, although higher selectivity can be obtained in some cases, most MMMs present an H_2/CH_4 separation performance below the 2008 upper bound.

As for CMS membranes, most of them show unprecedently high selectivity due to their effective molecule sieve effect. If their long-term stability and mechanical strength can be improved, needless to say, the CMS membranes will be the most competitive candidates for H_2/CH_4 separation.

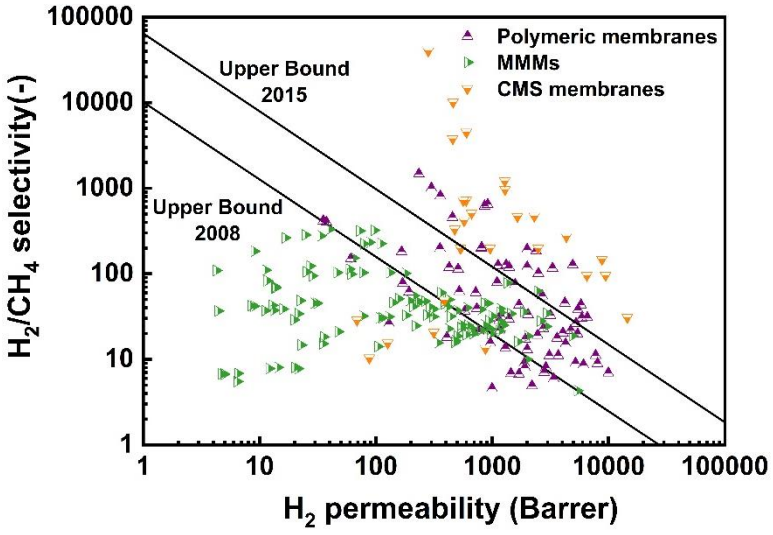

Figure 17. The comparison of H_2/CH_4 separation performance for polymeric membranes, MMMs and CMS membranes

6. Conclusions and perspectives

In this review, the recent progress of membranes for H_2/CH_4 separation has been summarized and analyzed, including polymeric membranes, MMMs and CMS membranes. Due to the relatively large difference in the molecule size between H_2 and CH_4, polymeric membranes, especially high free volume polymeric membranes, such as PIM-, TB polymer- and PI-based membranes, display superior H_2/CH_4 separation performances. However, physical aging and plasticization are two main bottlenecks for polymeric membranes before they can be applied in practical applications.

MMMs have also been widely explored for H_2/CH_4 separation. Many porous fillers,

including MOFs and PAFs, have been used as nanofillers in MMMs. Nonporous fillers such as CNTs were also reported. However, most MMMs have unsatisfying H_2/CH_4 separation performances that rarely approach or surpass the 2008 upper bound.

As an inorganic membrane, most CMS membranes revealed exceedingly supreme H_2 permeability and high H_2/CH_4 selectivity owing to its intrinsic molecular sieving effect. In most cases, CMS membranes with simultaneous high H_2 permeability and H_2/CH_4 selectivity can be obtained by optimizing the pyrolysis conditions as well as choosing a proper polymer as the precursor. However, seeking hydrophilic and flexible HF carbon membranes should be pursued to address the challenges of brittleness and physical aging.

According to the above-mentioned analysis of the literature data, membrane separation is a promising alternative for H_2/CH_4 separation. For future work, we present several perspectives on H_2/CH_4 separation membranes to inspire researchers interested in this topic:

(1) Developing membranes with both high permeability/permeance and high selectivity can significantly reduce the H_2/CH_4 separation cost. When selecting membrane materials, the potential of the membrane for large-scale production should also be considered. In addition, the economic feasibility of applying membranes for H_2/CH_4 separation should be also carried out.

(2) High free volume polymeric membranes have been documented with superior H_2/CH_4 separation performances. However, obvious physical aging was found for almost all the polymeric membranes. Finding a proper way to control or retard physical aging is critical for H_2/CH_4 separation membranes. In addition, the effects of plasticization on H_2/CH_4 separation membranes have rarely been reported; thus, improving the plasticization resistance of the polymeric membranes can be further studied.

(3) Compared to polymeric membranes, MMMs are less attractive in H_2/CH_4 separation. Yet, in some cases, adding a small amount of non-porous nanofillers have a significant positive effect on improving the mechanical properties of the membranes. Thus, this

method may have the potential to enhance membrane mechanical strength.

(4) CMS membranes are promising candidates for H_2/CH_4 separation due to the precise molecular sieving effect. More attention should be paid to improving the flexibility of CMS membranes while keeping their excellent separation property. On the other hand, the issue of separation performance loss due to physical aging should also be addressed, such as by applying efficient regeneration methods.

Abbreviations

Abbreviation	Full name
PIMs	polymers of intrinsic microporosity
TR polymer	thermally rearranged polymer
FFV	fractional free volume
t-Boc	tert-butoxycarbonyl
TB	Tröger's base
CANAL	catalytic arene-norbornene annulation
HTB	1,7-diamino-6H,12H-5,11-methanodibenzo[1,5]diazocine-2,8-diol
6FDA	4,4′-(hexafluoroisopropylidene)diphthalic anhydride
SBI	3,3,3′,3′-tetramethylspirobisindane-6,7,6′,7′-tetracarboxylic dianhydride
EA	ethanoanthracene
MP	methanopentacene
PIM-PIs	intrinsically microporous polyimides
CTB1	5,6,11,12-tetrahydro-5,11-methanodibenzo[a,e][8]annulene-2,3,8,9-tetracarboxylic anhydride
CTB2	6,12-dioxo-5,6,11,12-tetrahydro-5,11-methanodibenzo[a,e][8]annulene-2,3,8,9-tetracarboxylic dianhydride
DMN	dimethylnaphthidine
PBO	polybenzoxazoles
TC	thermal cyclodehydration

XRT	the crosslinked thermally rearranged polymer
FBN	functionalized boron nitride nanosheets
POXINARs	Poly(oxindolylidene arylene)s
PFMD	perfluoro-(2-methylene1,3-dioxolane)
CTFE	chlorotrifluoroethylene
PFMMD	perfluoro(2-methylene-4-methyl-1,3-dioxolane)
CMPs	conjugated microporous polymers
PSF	polysulfone
CP	coordination polymer
TrMCA	3,5-diamino-2,4,6-trimethylbenzoic acid
DAM	2,4,6- trimethyl-1,3-diaminobenzene
DABA	5-diaminobenzoic acid
dmbIm	5,6-dimethylbenzimidazole
PI	polyimide
ABA	4-aminobenzyl amine
PBDI	poly(p-phenylene benzobisimidazole)
IP	interfacial polymerization
TFCs	thin-film composites
CVD	chemical vapor deposition
DVB	divinylbenzene
MMMs	Mixed matrix membranes
PC	polycarbonates
CA	cellulose acetate
PEI	polyetherimide
PDMS	poly (dimethylsiloxane)
COFs	covalent organic frameworks
MOFs	metal-organic frameworks
CNT	carbon nanotubes
GO	graphene oxide
ZIFs	zeolitic imidazolate frameworks
PD	polydopamine
PHA	poly(hydroxyamide)
Co-BDC	Co-benzenedicarboxylate

MSSs	mesoporous silica MCM-41 spheres
ZTC	zeolite-templated carbon
PAFs	porous aromatic frameworks
HAB	3,3'-dihydroxyl-4,4'-diamino-biphenyl
DAM	2,4,6-trimethyl-m-phenylene
PGFs	porous graphitic frameworks
SWCNTs	single-walled carbon nanotubes
MWCNTs	multi-walled carbon nanotubes
TNT	titanium dioxide nanotube
PBNPI	poly(bisphenol A-co-4-nitrophthalic anhydride-co-1,3-phenylene diamine)
VIPS	vapor-induced phase separation
CMS	Carbon molecular sieve
ZCC	zeolite composite carbon
TBDA2	3,9-Diamino-4,10-dimethyl6H, 12H-5,11-methanodibenzo[1, 5]-diazocine
HPI	hydroxyl polyimide
PSM	postsynthetic modification
DMM	dimethoxymethane
Durene	2,3,5,6-tetramethyl-1,4-phenylenediamine
NMP	N-Methyl-2-pyrrolidone
ODA	4,4-oxydianiline
PTMSP	poly(1-trimethylsilyl-1-propyne)
SMR	steam methane reforming
CCS	carbon capture and storage
CG	coal gasification
BG	biomass gasification
CCUS	carbon capture, utilization and storage
PES	polyethersulfone

Acknowledgments

This work acknowledges the financial support from Sichuan Science and Technology

Program (2021YFH0116) and National Natural Science Foundation of China (No. 52170112).

References

1. Thuiller, W., *Climate change and the ecologist.* Nature, 2007. **448**(7153): p. 550-552.
2. Change, P.C.J.W.M.O., Geneva, Switzerland, *Global warming of 1.5 C.* 2018. **10**.
3. Mac Dowell, N., et al., *The role of CO2 capture and utilization in mitigating climate change.* Nature Climate Change, 2017. **7**(4): p. 243-249.
4. Yoro, K.O. and M.O. Daramola, *Chapter 1 - CO2 emission sources, greenhouse gases, and the global warming effect*, in *Advances in Carbon Capture*, M.R. Rahimpour, M. Farsi, and M.A. Makarem, Editors. 2020, Woodhead Publishing. p. 3-28.
5. COP25. *Climate Ambition Alliance*. 2022; Available from: https://cop25.mma.gob.cl/en/climate-ambition-alliance.
6. IEA, *An energy sector roadmap to carbon neutrality in China*. 2021, IEA: Paris.
7. Majava, A., et al., *Sectoral low-carbon roadmaps and the role of forest biomass in Finland's carbon neutrality 2035 target.* Energy Strategy Reviews, 2022. **41**: p. 100836.
8. IEA, *Global hydrogen demand by sector in the Sustainable Development Scenario, 2019-2070*. 2020: Paris.
9. Abdin, Z., et al., *Hydrogen as an energy vector.* Renewable and Sustainable Energy Reviews, 2020. **120**: p. 109620.
10. Nazir, H., et al., *Is the H2 economy realizable in the foreseeable future? Part I: H2 production methods.* International Journal of Hydrogen Energy, 2020. **45**(27): p. 13777-13788.
11. de Valladares, M.-R.J.I.E.A., *Global trends and outlook for hydrogen.* 2017.
12. Falcone, P.M., M. Hiete, and A. Sapio, *Hydrogen economy and sustainable development goals: Review and policy insights.* Current Opinion in Green and Sustainable Chemistry, 2021. **31**: p. 100506.
13. Al-Qahtani, A., et al., *Uncovering the true cost of hydrogen production routes using life cycle monetisation.* Applied Energy, 2021. **281**: p. 115958.
14. KPMG. *The hydrogen trajectory*. 2020; Available from: https://home.kpmg/xx/en/home/insights/2020/11/the-hydrogen-trajectory.html.
15. Nikolaidis, P. and A. Poullikkas, *A comparative overview of hydrogen production processes.* Renewable and Sustainable Energy Reviews, 2017. **67**: p. 597-611.
16. Martinez-Burgos, W.J., et al., *Hydrogen: Current advances and patented technologies of its renewable production.* Journal of Cleaner Production, 2021. **286**: p. 124970.
17. Zhou, R., et al., *Advanced microporous membranes for H2/CH4 separation:*

Challenges and perspectives. Advanced Membranes, 2021. **1**: p. 100011.

18. Sazali, N., *A comprehensive review of carbon molecular sieve membranes for hydrogen production and purification.* The International Journal of Advanced Manufacturing Technology, 2020. **107**(5): p. 2465-2483.
19. Mannan, H.A., et al., *Recent Applications of Polymer Blends in Gas Separation Membranes.* Chemical Engineering & Technology, 2013. **36**(11): p. 1838-1846.
20. Lau, C.H., et al., *Reverse-selective polymeric membranes for gas separations.* Progress in Polymer Science, 2013. **38**(5): p. 740-766.
21. Rezakazemi, M., et al., *State-of-the-art membrane based CO2 separation using mixed matrix membranes (MMMs): An overview on current status and future directions.* Progress in Polymer Science, 2014. **39**(5): p. 817-861.
22. Aroon, M.A., et al., *Performance studies of mixed matrix membranes for gas separation: A review.* Separation and Purification Technology, 2010. **75**(3): p. 229-242.
23. Li, H., et al., *Inorganic microporous membranes for H2 and CO2 separation—Review of experimental and modeling progress.* Chemical Engineering Science, 2015. **127**: p. 401-417.
24. Kim, S. and Y.M. Lee, *Rigid and microporous polymers for gas separation membranes.* Progress in Polymer Science, 2015. **43**: p. 1-32.
25. Zhang, C. and W.J. Koros, *Ultraselective Carbon Molecular Sieve Membranes with Tailored Synergistic Sorption Selective Properties.* Advanced Materials, 2017. **29**(33): p. 1701631.
26. Wang, Y., et al., *Amidoxime-grafted multiwalled carbon nanotubes by plasma techniques for efficient removal of uranium(VI).* Applied Surface Science, 2014. **320**: p. 10-20.
27. Alen, S.K., S. Nam, and S.A. Dastgheib, *Recent Advances in Graphene Oxide Membranes for Gas Separation Applications.* International Journal of Molecular Sciences, 2019. **20**(22).
28. Meshkat, S., S. Kaliaguine, and D. Rodrigue, *Mixed matrix membranes based on amine and non-amine MIL-53(Al) in Pebax® MH-1657 for CO2 separation.* Separation and Purification Technology, 2018. **200**: p. 177-190.
29. Dai, Z., L. Ansaloni, and L. Deng, *Recent advances in multi-layer composite polymeric membranes for CO2 separation: A review.* Green Energy & Environment, 2016. **1**(2): p. 102-128.
30. Sidhikku Kandath Valappil, R., N. Ghasem, and M. Al-Marzouqi, *Current and future trends in polymer membrane-based gas separation technology: A comprehensive review.* Journal of Industrial and Engineering Chemistry, 2021. **98**: p. 103-129.
31. Robeson, L.M., *The upper bound revisited.* Journal of Membrane Science, 2008. **320**(1): p. 390-400.
32. Freeman, B.D., *Basis of Permeability/Selectivity Tradeoff Relations in Polymeric Gas Separation Membranes.* Macromolecules, 1999. **32**(2): p. 375-380.
33. Budd, P.M., et al., *Polymers of intrinsic microporosity (PIMs): robust, solution-processable, organic nanoporous materials.* Chemical Communications,

2004(2): p. 230-231.
34. Budd, P.M., et al., *Gas separation membranes from polymers of intrinsic microporosity.* Journal of Membrane Science, 2005. **251**(1): p. 263-269.
35. Thomas, S., et al., *Pure- and mixed-gas permeation properties of a microporous spirobisindane-based ladder polymer (PIM-1).* Journal of Membrane Science, 2009. **333**(1): p. 125-131.
36. Mizrahi Rodriguez, K., et al., *Leveraging Free Volume Manipulation to Improve the Membrane Separation Performance of Amine-Functionalized PIM-1.* Angewandte Chemie International Edition, 2021. **60**(12): p. 6593-6599.
37. He, S., et al., *Intermediate thermal manipulation of polymers of intrinsic microporous (PIMs) membranes for gas separations.* AIChE Journal, 2020. **66**(10): p. e16543.
38. Huang, M., et al., *Thermally Cross-Linked Amidoxime-Functionalized Polymers of Intrinsic Microporosity Membranes for Highly Selective Hydrogen Separation.* ACS Sustainable Chemistry & Engineering, 2021. **9**(28): p. 9426-9435.
39. Lai Holden, W.H., et al., *Hydrocarbon ladder polymers with ultrahigh permselectivity for membrane gas separations.* Science, 2022. **375**(6587): p. 1390-1392.
40. Wang, Y., et al., *Recent Progress on Polymers of Intrinsic Microporosity and Thermally Modified Analogue Materials for Membrane-Based Fluid Separations.* Small Structures, 2021. **2**(9): p. 2100049.
41. Swaidan, R., B. Ghanem, and I. Pinnau, *Fine-Tuned Intrinsically Ultramicroporous Polymers Redefine the Permeability/Selectivity Upper Bounds of Membrane-Based Air and Hydrogen Separations.* ACS Macro Letters, 2015. **4**(9): p. 947-951.
42. Low, Z.-X., et al., *Gas Permeation Properties, Physical Aging, and Its Mitigation in High Free Volume Glassy Polymers.* Chemical Reviews, 2018. **118**(12): p. 5871-5911.
43. Ma, X., et al., *Unprecedented gas separation performance of a difluoro-functionalized triptycene-based ladder PIM membrane at low temperature.* Journal of Materials Chemistry A, 2021. **9**(9): p. 5404-5414.
44. Zhu, Z., et al., *Enhanced Gas Separation Properties of Tröger's Base Polymer Membranes Derived from Pure Triptycene Diamine Regioisomers.* Macromolecules, 2020. **53**(5): p. 1573-1584.
45. Ma, X., et al., *Facile Synthesis and Study of Microporous Catalytic Arene-Norbornene Annulation–Tröger's Base Ladder Polymers for Membrane Air Separation.* ACS Macro Letters, 2020. **9**(5): p. 680-685.
46. Carta, M., et al., *An Efficient Polymer Molecular Sieve for Membrane Gas Separations.* Science, 2013. **339**(6117): p. 303-307.
47. Carta, M., et al., *Triptycene Induced Enhancement of Membrane Gas Selectivity for Microporous Tröger's Base Polymers.* Advanced Materials, 2014. **26**(21): p. 3526-3531.
48. Rose, I., et al., *Highly Permeable Benzotriptycene-Based Polymer of Intrinsic Microporosity.* ACS Macro Letters, 2015. **4**(9): p. 912-915.

49. Williams, R., et al., *A highly rigid and gas selective methanopentacene-based polymer of intrinsic microporosity derived from Tröger's base polymerization.* Journal of Materials Chemistry A, 2018. **6**(14): p. 5661-5667.
50. Rose, I., et al., *Polymer ultrapermeability from the inefficient packing of 2D chains.* Nature Materials, 2017. **16**(9): p. 932-937.
51. Chen, X., et al., *Ultra-selective molecular-sieving gas separation membranes enabled by multi-covalent-crosslinking of microporous polymer blends.* Nature Communications, 2021. **12**(1): p. 6140.
52. Yoshioka, T., et al., *Gas-separation properties of amine-crosslinked polyimide membranes modified by amine vapor.* Journal of Applied Polymer Science, 2017. **134**(10).
53. Ma, X., et al., *Facile Synthesis of a Hydroxyl-Functionalized Tröger's Base Diamine: A New Building Block for High-Performance Polyimide Gas Separation Membranes.* Macromolecules, 2017. **50**(24): p. 9569-9576.
54. Ma, X., M.A. Abdulhamid, and I. Pinnau, *Design and Synthesis of Polyimides Based on Carbocyclic Pseudo-Tröger's Base-Derived Dianhydrides for Membrane Gas Separation Applications.* Macromolecules, 2017. **50**(15): p. 5850-5857.
55. Abdulhamid, M.A., et al., *Plasticization-Resistant Carboxyl-Functionalized 6FDA-Polyimide of Intrinsic Microporosity (PIM-PI) for Membrane-Based Gas Separation.* Industrial & Engineering Chemistry Research, 2020. **59**(12): p. 5247-5256.
56. Luo, S., et al., *Preparation and gas transport properties of triptycene-containing polybenzoxazole (PBO)-based polymers derived from thermal rearrangement (TR) and thermal cyclodehydration (TC) processes.* Journal of Materials Chemistry A, 2016. **4**(43): p. 17050-17062.
57. Luo, S., et al., *Highly Selective and Permeable Microporous Polymer Membranes for Hydrogen Purification and CO2 Removal from Natural Gas.* Chemistry of Materials, 2018. **30**(15): p. 5322-5332.
58. Shao, P., et al., *Molecular-Sieving Membrane by Partitioning the Channels in Ultrafiltration Membrane by In Situ Polymerization.* Angewandte Chemie International Edition, 2020. **59**(11): p. 4401-4405.
59. Mancilla, E.C., et al., *POXINAR Membrane Family for Gas Separation.* Industrial & Engineering Chemistry Research, 2019. **58**(33): p. 15280-15287.
60. Park Ho, B., et al., *Polymers with Cavities Tuned for Fast Selective Transport of Small Molecules and Ions.* Science, 2007. **318**(5848): p. 254-258.
61. Wang, Y., et al., *Functionalized Boron Nitride Nanosheets: A Thermally Rearranged Polymer Nanocomposite Membrane for Hydrogen Separation.* Angewandte Chemie International Edition, 2018. **57**(49): p. 16056-16061.
62. Han, S.H., et al., *Tuning microcavities in thermally rearranged polymer membranes for CO2 capture.* Physical Chemistry Chemical Physics, 2012. **14**(13): p. 4365-4373.
63. Li, S., et al., *Mechanically robust thermally rearranged (TR) polymer membranes with spirobisindane for gas separation.* Journal of Membrane Science, 2013. **434**: p. 137-147.

64. Zhuang, Y., et al., *Intrinsically Microporous Soluble Polyimides Incorporating Tröger's Base for Membrane Gas Separation.* Macromolecules, 2014. **47**(10): p. 3254-3262.
65. Fang, M., et al., *High-performance perfluorodioxolane copolymer membranes for gas separation with tailored selectivity enhancement.* Journal of Materials Chemistry A, 2018. **6**(2): p. 652-658.
66. Shan, M., et al., *Novel high performance poly(p-phenylene benzobisimidazole) (PBDI) membranes fabricated by interfacial polymerization for H2 separation.* Journal of Materials Chemistry A, 2019. **7**(15): p. 8929-8937.
67. Okamoto, Y., et al., *New amorphous perfluoro polymers: perfluorodioxolane polymers for use as plastic optical fibers and gas separation membranes.* Polymers for Advanced Technologies, 2016. **27**(1): p. 33-41.
68. Villalobos Luis, F., et al., *Large-scale synthesis of crystalline g-C3N4 nanosheets and high-temperature H2 sieving from assembled films.* Science Advances. **6**(4): p. eaay9851.
69. Lee, J., et al., *Ultrathin Water-Cast Polymer Membranes for Hydrogen Purification.* ACS Applied Materials & Interfaces, 2022. **14**(5): p. 7292-7300.
70. Kargari, A., A. Arabi Shamsabadi, and M. Bahrami Babaheidari, *Influence of coating conditions on the H2 separation performance from H2/CH4 gas mixtures by the PDMS/PEI composite membrane.* International Journal of Hydrogen Energy, 2014. **39**(12): p. 6588-6597.
71. Boscher, N.D., M. Wang, and K.K. Gleason, *Chemical vapour deposition of metalloporphyrins: a simple route towards the preparation of gas separation membranes.* Journal of Materials Chemistry A, 2016. **4**(46): p. 18144-18152.
72. Baker, R.W., *Membrane technology and applications*. 2012: John Wiley & Sons.
73. Goh, P.S., et al., *Recent advances of inorganic fillers in mixed matrix membrane for gas separation.* Separation and Purification Technology, 2011. **81**(3): p. 243-264.
74. Kamble, A.R., C.M. Patel, and Z.V.P. Murthy, *A review on the recent advances in mixed matrix membranes for gas separation processes.* Renewable and Sustainable Energy Reviews, 2021. **145**: p. 111062.
75. Ahmad, A.L., et al., *A cellulose acetate/multi-walled carbon nanotube mixed matrix membrane for CO2/N2 separation.* Journal of Membrane Science, 2014. **451**: p. 55-66.
76. Galizia, M., et al., *50th Anniversary Perspective: Polymers and Mixed Matrix Membranes for Gas and Vapor Separation: A Review and Prospective Opportunities.* Macromolecules, 2017. **50**(20): p. 7809-7843.
77. Nasir, R., et al., *Material Advancements in Fabrication of Mixed-Matrix Membranes.* Chemical Engineering & Technology, 2013. **36**(5): p. 717-727.
78. Kang, Z., et al., *Mixed Matrix Membranes (MMMs) Comprising Exfoliated 2D Covalent Organic Frameworks (COFs) for Efficient CO2 Separation.* Chemistry of Materials, 2016. **28**(5): p. 1277-1285.
79. Chung, T.-S., et al., *Mixed matrix membranes (MMMs) comprising organic polymers with dispersed inorganic fillers for gas separation.* Progress in

Polymer Science, 2007. **32**(4): p. 483-507.
80. Vinoba, M., et al., *Recent progress of fillers in mixed matrix membranes for CO2 separation: A review.* Separation and Purification Technology, 2017. **188**: p. 431-450.
81. Lin, R., et al., *Metal organic framework based mixed matrix membranes: an overview on filler/polymer interfaces.* Journal of Materials Chemistry A, 2018. **6**(2): p. 293-312.
82. Wang, Y., et al., *110th Anniversary: Mixed Matrix Membranes with Fillers of Intrinsic Nanopores for Gas Separation.* Industrial & Engineering Chemistry Research, 2019. **58**(19): p. 7706-7724.
83. Ahmadi, M., et al., *Performance of Mixed Matrix Membranes Containing Porous Two-Dimensional (2D) and Three-Dimensional (3D) Fillers for CO2 Separation: A Review.* Membranes, 2018. **8**(3).
84. Yaumi, A.L., M.Z.A. Bakar, and B.H. Hameed, *Recent advances in functionalized composite solid materials for carbon dioxide capture.* Energy, 2017. **124**: p. 461-480.
85. Zhou, H.C., J.R. Long, and O.M. Yaghi, *Introduction to Metal-Organic Frameworks.* CHEMICAL REVIEWS, 2012. **112**(2): p. 673-674.
86. Wu, T., et al., *Separation Performance of Si-CHA Zeolite Membrane for a Binary H2/CH4 Mixture and Ternary and Quaternary Mixtures Containing Impurities.* Energy & Fuels, 2020. **34**(9): p. 11650-11659.
87. *Introduction to Metal - Organic Frameworks.* Chemical Reviews, 2012. **112**(2): p. 673-674.
88. Wang, Z., et al., *Interfacial Design of Mixed Matrix Membranes for Improved Gas Separation Performance.* Advanced Materials, 2016. **28**(17): p. 3399-3405.
89. Kim, J.S., et al., *Mixed matrix membranes with a thermally rearranged polymer and ZIF-8 for hydrogen separation.* Journal of Membrane Science, 2019. **582**: p. 381-390.
90. Japip, S., S. Erifin, and T.-S. Chung, *Reduced thermal rearrangement temperature via formation of zeolitic imidazolate framework (ZIF)-8-based nanocomposites for hydrogen purification.* Separation and Purification Technology, 2019. **212**: p. 965-973.
91. Yuan, S.H., et al., *Nanosized Core - Shell Zeolitic Imidazolate Frameworks-Based Membranes for Gas Separation.* Small Methods, 2020. **4**(8): p. 2000021.
92. Fan, Y., et al., *Zn(II)-modified imidazole containing polyimide/ZIF-8 mixed matrix membranes for gas separations.* Journal of Membrane Science, 2020. **597**: p. 117775.
93. Safak Boroglu, M. and A.B. Yumru, *Gas separation performance of 6FDA-DAM-ZIF-11 mixed-matrix membranes for H2/CH4 and CO2/CH4 separation.* Separation and Purification Technology, 2017. **173**: p. 269-279.
94. Safak Boroglu, M., I. Boz, and B. Kaya, *Effect of new metal - organic framework (zeolitic imidazolate framework [ZIF-12]) in mixed matrix membranes on structure, morphology, and gas separation properties.* Journal of Polymer Engineering, 2021. **41**(4): p. 259-270.

95. Ghanem, A.S., et al., *High gas permselectivity in ZIF-302/polyimide self-consistent mixed-matrix membrane.* Journal of Applied Polymer Science, 2020. **137**(13): p. 48513.
96. Zhang, Q., et al., *Preparation and gas separation performance of mixed-matrix membranes based on triptycene-containing polyimide and zeolite imidazole framework (ZIF-90).* Polymer, 2017. **131**: p. 209-216.
97. Al-Maythalony, B.A., et al., *Tuning the Interplay between Selectivity and Permeability of ZIF-7 Mixed Matrix Membranes.* ACS Applied Materials & Interfaces, 2017. **9**(39): p. 33401-33407.
98. Deng, J., Z. Dai, and L. Deng, *H2-selective Troger's base polymer based mixed matrix membranes enhanced by 2D MOFs.* Journal of Membrane Science, 2020. **610**: p. 118262.
99. Kim, E.Y., et al., *Preparation of Mixed Matrix Membranes Containing ZIF-8 and UiO-66 for Multicomponent Light Gas Separation.* Crystals, 2019. **9**(1).
100. Wang, Z., et al., *Constructing Strong Interfacial Interactions under Mild Conditions in MOF-Incorporated Mixed Matrix Membranes for Gas Separation.* ACS Applied Materials & Interfaces, 2021. **13**(2): p. 3166-3174.
101. Ma, C. and J.J. Urban, *Hydrogen-Bonded Polyimide/Metal-Organic Framework Hybrid Membranes for Ultrafast Separations of Multiple Gas Pairs.* Advanced Functional Materials, 2019. **29**(32): p. 1903243.
102. Ma, C. and J.J. Urban, *Enhanced CO2 Capture and Hydrogen Purification by Hydroxy Metal-Organic Framework/Polyimide Mixed Matrix Membranes.* ChemSusChem, 2019. **12**(19): p. 4405-4411.
103. Smith, Z.P., et al., *Increasing M2(dobdc) Loading in Selective Mixed-Matrix Membranes: A Rubber Toughening Approach.* Chemistry of Materials, 2018. **30**(5): p. 1484-1495.
104. Bi, X., et al., *MOF Nanosheet-Based Mixed Matrix Membranes with Metal-Organic Coordination Interfacial Interaction for Gas Separation.* ACS Applied Materials & Interfaces, 2020. **12**(43): p. 49101-49110.
105. Zornoza, B., et al., *Mixed matrix membranes based on 6FDA polyimide with silica and zeolite microsphere dispersed phases.* AIChE Journal, 2015. **61**(12): p. 4481-4490.
106. Gunawan, T., et al., *The utilization of micro-mesoporous carbon-based filler in the P84 hollow fibre membrane for gas separation.* Royal Society Open Science. **8**(2): p. 201150.
107. Wijiyanti, R., et al., *Enhanced gas separation performance of polysulfone membrane by incorporation of zeolite-templated carbon.* MALAYSIAN JOURNAL OF FUNDAMENTAL AND APPLIED SCIENCES, 2020. **16**(2): p. 128-134.
108. Smith, S.J.D., et al., *Highly permeable Thermally Rearranged Mixed Matrix Membranes (TR-MMM).* Journal of Membrane Science, 2019. **585**: p. 260-270.
109. Hou, R., et al., *Highly permeable and selective mixed-matrix membranes for hydrogen separation containing PAF-1.* Journal of Materials Chemistry A, 2020. **8**(29): p. 14713-14720.
110. Ma, C., et al., *Pyrazine-Fused Porous Graphitic Framework-Based Mixed Matrix*

Membranes for Enhanced Gas Separations. ACS Applied Materials & Interfaces, 2020. **12**(14): p. 16922-16929.

111. Carter, D., et al., *Investigation and comparison of mixed matrix membranes composed of polyimide matrimid with ZIF - 8, silicalite, and SAPO - 34.* Journal of Membrane Science, 2017. **544**: p. 35-46.

112. Ma, X., et al., *Polymer Composite Membrane with Penetrating ZIF-7 Sheets Displays High Hydrogen Permselectivity.* Angewandte Chemie International Edition, 2019. **58**(45): p. 16156-16160.

113. Hayashi, H., et al., *Zeolite A imidazolate frameworks.* Nature Materials, 2007. **6**(7): p. 501-506.

114. Deng, J., Z. Dai, and L. Deng, *Effects of the Morphology of the ZIF on the CO2 Separation Performance of MMMs.* Industrial & Engineering Chemistry Research, 2020. **59**(32): p. 14458-14466.

115. Zheng, W., et al., *ZIF-8 nanoparticles with tunable size for enhanced CO2 capture of Pebax based MMMs.* Separation and Purification Technology, 2019. **214**: p. 111-119.

116. Cavka, J.H., et al., *A New Zirconium Inorganic Building Brick Forming Metal Organic Frameworks with Exceptional Stability.* Journal of the American Chemical Society, 2008. **130**(42): p. 13850-13851.

117. Ben, T., et al., *Targeted Synthesis of a Porous Aromatic Framework with High Stability and Exceptionally High Surface Area.* Angewandte Chemie International Edition, 2009. **48**(50): p. 9457-9460.

118. Regmi, C., et al., *CO2/CH4 and H2/CH4 Gas Separation Performance of CTA-TNT@CNT Hybrid Mixed Matrix Membranes.* Membranes, 2021. **11**(11).

119. Weng, T.-H., H.-H. Tseng, and M.-Y. Wey, *Preparation and characterization of multi-walled carbon nanotube/PBNPI nanocomposite membrane for H2/CH4 separation.* International Journal of Hydrogen Energy, 2009. **34**(20): p. 8707-8715.

120. Ghomshani, A.D., et al., *Improvement of H2/CH4 Separation Performance of PES Hollow Fiber Membranes by Addition of MWCNTs into Polymeric Matrix.* Polymer-Plastics Technology and Engineering, 2016. **55**(11): p. 1155-1166.

121. Sajjan, P., et al., *Fabrication of Cellulose Acetate Film through Blending Technique with Palladium Acetate for Hydrogen Gas Separation.* Energy & Fuels, 2020. **34**(9): p. 11699-11707.

122. Ruan, S.L., et al., *Toughening high performance ultrahigh molecular weight polyethylene using multiwalled carbon nanotubes.* Polymer, 2003. **44**(19): p. 5643-5654.

123. Nejad, M.N., M. Asghari, and M. Afsari, *Investigation of Carbon Nanotubes in Mixed Matrix Membranes for Gas Separation: A Review.* ChemBioEng Reviews, 2016. **3**(6): p. 276-298.

124. Ismail, A.F., et al., *A REVIEW OF PURIFICATION TECHNIQUES FOR CARBON NANOTUBES.* Nano, 2008. **03**(03): p. 127-143.

125. Skoulidas, A.I., et al., *Rapid Transport of Gases in Carbon Nanotubes.* Physical Review Letters, 2002. **89**(18): p. 185901.

126. Yousef, S., et al., *Ultra-permeable CNTs/PES membranes with a very low CNTs content and high H2/N2 and CH4/N2 selectivity for clean energy extraction applications.* Journal of Materials Research and Technology, 2021. **15**: p. 5114-5127.
127. He, X. and I. Kumakiri, *Carbon Membrane Technology: Fundamentals and Applications*. 2020: CRC Press.
128. Lei, L., et al., *Carbon membranes for CO2 removal: Status and perspectives from materials to processes.* Chemical Engineering Journal, 2020. **401**: p. 126084.
129. Sazali, N., *A review of the application of carbon-based membranes to hydrogen separation.* Journal of Materials Science, 2020. **55**(25): p. 11052-11070.
130. Widiastuti, N., et al., *Development of a P84/ZCC Composite Carbon Membrane for Gas Separation of H2/CO2 and H2/CH4.* ACS Omega, 2021. **6**(24): p. 15637-15650.
131. Wang, Z., et al., *Carbon Molecular Sieve Membranes Derived from Tröger's Base-Based Microporous Polyimide for Gas Separation.* ChemSusChem, 2018. **11**(5): p. 916-923.
132. Liang, J., et al., *Effects on Carbon Molecular Sieve Membrane Properties for a Precursor Polyimide with Simultaneous Flatness and Contortion in the Repeat Unit.* ChemSusChem, 2020. **13**(20): p. 5531-5538.
133. Lei, L., et al., *Carbon hollow fiber membranes for a molecular sieve with precise-cutoff ultramicropores for superior hydrogen separation.* Nature Communications, 2021. **12**(1): p. 268.
134. Liu, J., et al., *Self-standing permselective CMS membrane from melt extruded PVDC.* Journal of Membrane Science, 2020. **615**: p. 118554.
135. Llosa Tanco, M.A. and D.A. Pacheco Tanaka, *Recent Advances on Carbon Molecular Sieve Membranes (CMSMs) and Reactors.* Processes, 2016. **4**(3).
136. Tseng, H.-H., et al., *Enhanced H2/CH4 and H2/CO2 separation by carbon molecular sieve membrane coated on titania modified alumina support: Effects of TiO2 intermediate layer preparation variables on interfacial adhesion.* Journal of Membrane Science, 2016. **510**: p. 391-404.
137. Wey, M.-Y., et al., *Interfacial interaction between CMS layer and substrate: Critical factors affecting membrane microstructure and H2 and CO2 separation performance from CH4.* Journal of Membrane Science, 2019. **580**: p. 49-61.
138. Lin, Y.-T., et al., *Insights into the Role of Polymer Conformation on the Cutoff Size of Carbon Molecular Sieving Membranes for Hydrogen Separation and Its Novel Pore Size Detection Technology.* ACS Applied Materials & Interfaces, 2021. **13**(4): p. 5165-5175.
139. Nordio, M.L.V., et al., *Water Adsorption Effect on Carbon Molecular Sieve Membranes in H2-CH4 Mixture at High Pressure.* Energies, 2020. **13**(14).